

The Role of Dust in Models of Population Synthesis

L. P. Cassarà^{1,2*}, L. Piovan^{1,3*}, A. Weiss^{3*}, M. Salaris^{4*} and C. Chiosi^{1*}

¹*Department of Physics and Astronomy, University of Padova, Via Marzolo 8-I, 35131, Padova, Italy*

²*INAF-IASF Milano, Via E. Bassini 15, 20133 Milano, Italy*

³*Max-Planck-Institut für Astrophysik, Karl-Schwarzschild-Str. 1, Garching bei München, Germany*

⁴*Astrophysics Research Institute, Liverpool John Moores University, IC2, Liverpool Science Park, United Kingdom*

Accepted 2013 September 19. Received 2013 September 18; in original form 2013 June 15

ABSTRACT

We have employed state-of-the-art evolutionary models of low and intermediate-mass AGB stars, and included the effect of circumstellar dust shells on the spectral energy distribution (SED) of AGB stars, to revise the Padua library of isochrones (Bertelli et al. 1994) that covers an extended range of ages and initial chemical compositions. The major revision involves the thermally pulsing AGB phase, that is now taken from fully evolutionary calculations by Weiss & Ferguson (2009). Two libraries of about 600 AGB dust-enshrouded SEDs each, have also been calculated, one for oxygen-rich M-stars and one for carbon-rich C-stars. Each library accounts for different values of input parameters like the optical depth τ , dust composition, and temperature of the inner boundary of the dust shell. These libraries of dusty AGB spectra have been implemented into a large composite library of theoretical stellar spectra, to cover all regions of the Hertzsprung-Russell Diagram (HRD) crossed by the isochrones.

With the aid of the above isochrones and libraries of stellar SEDs, we have calculated the spectro-photometric properties (SEDs, magnitudes, and colours) of single-generation stellar populations (SSPs) for six metallicities, more than fifty ages (from ~ 3 Myr to 15 Gyr), and nine choices of the Initial Mass Function. The new isochrones and SSPs have been compared to the colour-magnitude diagrams (CMDs) of field populations in the LMC and SMC, with particular emphasis on AGB stars, and the integrated colours of star clusters in the same galaxies, using data from the SAGE (*Surveying the Agents of Galaxy Evolution*) catalogues. We have also examined the integrated colours of a small sample of star clusters located in the outskirts of M31. The agreement between theory and observations is generally good. In particular, the new SSPs reproduce the red tails of the AGB star distribution in the CMDs of field stars in the Magellanic Clouds. Some discrepancies still exist and need to be investigated further.

Key words: stars: AGB and post-AGB – circumstellar matter – Hertzsprung–Russell and colour–magnitude diagrams – infrared: stars – Magellanic Clouds – radiative transfer.

1 INTRODUCTION

The frontier for high- z objects has been continuously and quickly extended by the HST WFC3 camera from $z \sim 4$ –5 (Madau et al. 1996; Steidel et al. 1999), and $z \sim 6$ (Stanway, Bunker & McMahon 2003; Dickinson et al. 2004) to $z \sim 10$ (Zheng et al. 2012; Bouwens et al. 2012;

Oesch et al. 2012).

According to the current view, first galaxies formed at $z \sim 10$ –20 (Rowan-Robinson 2012), and this high redshift universe is obscured by copious amounts of dust (see Shapley et al. 2001; Carilli et al. 2001; Robson et al. 2004; Wang et al. 2008a,b; Michałowski, Watson & Hjorth 2010; Michałowski et al. 2010), whose origin and composition are a matter of debate (Gall, Andersen & Hjorth 2011a,b; Dwek, Galliano & Jones 2009; Draine 2009; Dwek & Cherchneff 2011). Understanding the properties of this interstellar dust, and modelling its coupling with

* E-mail: letizia@lambrate.inaf.it (LPC);
lorenzo.piovan@gmail.com (LP); weiss@mpa-garching.mpg.de (AW); M.Salaris@ljmu.ac.uk (MS); cesare.chiosi@unipd.it (CC)

stellar populations are critical to determine the properties of the high- z universe, and obtain precious clues on the fundamental question of when and how galaxies formed and evolved. A major effort is thus being made in the theoretical spectro-photometric, dynamical, and chemical modelling of dusty galaxies (see for instance Narayanan et al. 2010; Jonsson, Groves & Cox 2010; Grassi et al. 2010; Pipino et al. 2011; Popescu et al. 2011). Stellar radiation is absorbed by dust, and reemitted at longer wavelengths, resulting in a change of its spectral energy distribution (SED) (Silva et al. 1998; Piovan, Tantalo & Chiosi 2006b; Popescu et al. 2011). Dust also strongly affects the production of molecular hydrogen and the local amount of UV radiation in galaxies, thus playing a major role in the star formation process (Yamasawa et al. 2011).

The inclusion of dust in the theoretical models of galaxy spectra leads to a growing complexity and typically to a much larger set of parameters. We can identify two main circumstances in which dust interacts with the stellar light. First, massive stars are embedded in their parental molecular clouds (MCs), during the early evolution; the duration of this phase is short, but the effect of dust on the stellar spectra is not negligible, and a significant fraction of light is shifted to the IR region. Second, during the asymptotic giant branch (AGB) phase low and intermediate mass stars may form an outer dust-rich shell of material, that obscures and reprocesses the radiation emitted from the photosphere.

Stars and dust are tightly interwoven not only *locally* (stars-MCs, stars-circumstellar dust shell), but also *globally* (stars, gas and dust mixed in the galactic environment). In general, dust is partly associated with the diffuse interstellar medium (ISM), partly with star forming molecular regions, and partly with the circumstellar envelopes of AGB stars. In all cases, the effect is the absorption of the stellar light at UV-optical wavelength, with consequent re-emission in the NIR-MIR-FIR (near, middle and far infrared, respectively). It is clear from these considerations that dust affects the observed SEDs of high- z objects, hampering their interpretation in terms of fundamental physical parameters like stellar ages, metallicities, initial mass function (IMF), and the determination of the galaxy star formation histories (SFHs).

This paper is the first of a series devoted to study the spectro-photometric evolution of star clusters and galaxies, taking into account the key role played by dust in determining the spectro-photometric properties of single-generation stellar populations (SSPs). The final goal is to derive new state-of-the-art isochrones and integrated properties of SSPs, and to model the spectro-photometric properties of galaxies, considering the local and global effects of dust formation, destruction and evolution.

We have set up an extended library of isochrones and SSPs of different chemical composition, age and IMFs, that take into account the effect of circumstellar dust around AGB stars. Although we will show that the IMF has a marginal effect on the SED, hence magnitudes and colours of SSPs, it plays an important role in determining properties of galaxies, that can be interpreted as the sum of many SSPs of different age, weighted by the SFH. In fact, the IMF affects both the chemical enrichment of the

galactic ISM by the stellar ejecta, and the galaxy stellar mass.

The outline of the paper is as follows. Section 2 provides a brief review of the state-of-the art regarding theoretical isochrones and SSPs, the building blocks of the evolutionary population synthesis (EPS) models. In Section 3 we describe the new models for AGB stars by Weiss & Ferguson (2009) and how they have been included in the Padua Library of stellar models and isochrones by Bertelli et al. (1994). Section 4 presents our new isochrones, whereas in Section 5 we describe the companion SSPs without the inclusion of dust. Section 6 analyzes the effects of dust shells around AGB stars on the radiation emitted by the central object. In particular, we model the dust-rich envelope of AGB stars at varying optical depth, as a function of the efficiency of mass-loss and the dust to gas ratio. We finally calculate two libraries of stellar spectra for oxygen-rich M-type stars and carbon-rich C-stars, respectively. The results are described in Section 7. The SSPs including the effect of dust, are presented in Section 8. In Section 9, we validate our isochrones and SSPs on Small and Large Magellanic Cloud (SMC and LMC) field stars, and clusters in the SMC, LMC and M31. Finally, Section 10, summarizes the main results of this study.

2 ISOCHRONES WITH AGB STARS

Stellar evolutionary tracks, isochrones and SSPs can be used to study photometric and spectroscopic observations of resolved and unresolved stellar populations, from the simple age-dating of star clusters, to the derivation of star formation histories of resolved galaxies. To mention just a few recent applications, we recall here Pessev et al. (2006, 2008), Ma (2012) and references therein.

They are also necessary to study the spectro-photometric evolution of galaxies, using either EPS classical models (Arimoto & Yoshii 1987; Bressan, Chiosi & Fagotto 1994; Silva et al. 1998; Buzzoni 2002; Bruzual & Charlot 2003; Buzzoni 2005; Piovan, Tantalo & Chiosi 2006b), or models based on chemo-dynamical simulations, like the ones presented in Tantalo et al. (2010). For a recent review of the EPS theory, see, e.g., Conroy (2013).

Many groups have published large grids of stellar isochrones, covering a wide range of stellar parameters (age, mass, metal content, metal mixture, helium abundance) that can be used in stellar population synthesis models of galaxies. To give just a few examples, we refer the reader to the Geneva database of stellar evolution tracks and isochrones (Lejeune & Schaerer 2001), the various releases of stellar tracks and isochrones from Padua (Bertelli et al. 1994; Girardi et al. 2002; Marigo et al. 2008; Bertelli et al. 2008), the BaSTI database (Pietrinferni et al. 2004, 2006; Cordier et al. 2007), the Dartmouth database (Dotter et al. 2008), the Yunnan-I (Zhang et al. 2002), Yunnan-II (Zhang et al. 2004, 2005) and most recently the Yunnan-III models (Zhang et al. 2012). A more detailed overview is given by Zhang et al. (2012) and will not be repeated here.

One of the major uncertainties is the inclusion of the AGB evolutionary phase. In brief, AGB stars play an important role for populations with an age larger than

about one hundred million years. Even though the AGB phase is short lived, these stars are very bright, they may reach very low effective temperatures, and can get enshrouded in a shell of self-produced dust that reprocesses the radiation emitted by the central object. Thanks to their luminosity, they contribute significantly to the total light emitted by a SSP. Also, because of their low surface temperatures, they dominate the NIR spectra and colours. All stars in the mass range from about $0.8 M_{\odot}$ to $\sim 6 M_{\odot}$, are known to become AGB stars towards the end of their evolution, before moving to the Planetary Nebula (PN) and carbon-oxygen White Dwarf (CO-WD) phases, after having lost their envelope. The AGB phase is characterized by the so-called thermal pulsing instability of the He-burning shell (TP-AGB phase) that causes recurrent expansions/contractions of the envelope and other surface phenomena that make the AGB phase particularly difficult to follow. There are currently two classes of models for the TP-AGB phase. The first one includes the semi-analytical or synthetic TP-AGB models; these calculations model the evolution of the layers above the inert CO-core, by adopting suitable inner boundary conditions, and account for mass-loss from the photosphere and envelope burning (EB; also called Hot Bottom Burning HBB). By employing analytical relations obtained from fully evolutionary calculations regarding, i.e., the CO-core mass-luminosity relation, the evolution through the thermal pulses is followed, taking into account the growth of the CO-core, the change of the surface abundances, its effect on the surface opacities, the decrease of the total mass, and the increase of the mean luminosity (see Marigo, Bressan & Chiosi 1996; Wagenhuber & Groenewegen 1998; Marigo, Bressan & Chiosi 1998; Marigo 2002; Izzard et al. 2004; Cordier et al. 2007; Marigo & Girardi 2007; Buell 2012, and references therein). The second type of models includes time-consuming, full evolutionary AGB calculations (Karakas, Lattanzio & Pols 2002; Straniero et al. 2003; Kitsikis & Weiss 2007; Weiss & Ferguson 2009; Karakas 2011). Additionally, models can be grouped according to the opacity adopted for the outer layers, e.g. opacities with fixed carbon to oxygen abundance ratio (denoted here as $[C/O]$, with $[C/O] < 1$ typical of the envelopes of M-stars), and opacities dependent on $[C/O]$, that can increase above unity as the abundance of carbon increases during the third dredge-up.

The old past: short AGB tracks. We consider the isochrones of Bertelli et al. (1994) to illustrate the past situation with classical models of AGB stars, i.e. synthetic models with envelope opacities for $[C/O]$ -ratios typical of M-stars. The points to note are (i) the limited redward extension of the AGB in the HR diagram (HRD), due to the low opacity in the C-O-rich envelopes of these stars (see Marigo 2002, and below); (ii) isochrones (and SSPs in turn) of metallicity significantly higher than solar (e.g. $Z=0.05$ and $Z=0.1$) miss the AGB phase and directly evolve from core He-burning to the White Dwarf WD stage. Stars of this type are good candidates to explain the UV-excess of elliptical galaxies and its correlation with metallicity (Bressan, Chiosi & Fagotto 1994). In brief: low mass stars (and stars at the lower end of the intermediate-mass range) with metallicities $\sim 2.5 Z_{\odot}$ un-

dergo the He-burning at the red side of their HB (red-HB) but miss the TP-AGB. Soon after the early-AGB (E-AGB) phase is completed, they move to the WD stage. When the metallicity is higher, ($3 Z_{\odot}$), low-mass He-burning stars ($0.55 - 0.6 M_{\odot}$) spend a significant fraction of their evolution at rather high T_{eff} , and soon after He-exhaustion in the core, they evolve directly to the WD stage. They are called Hot-HB and AGB-manqué objects, and play a crucial role in the UV-upturn of massive elliptical galaxies (Greggio & Renzini 1990; Castellani & Tornambe 1991; Bressan, Chiosi & Fagotto 1994). This behaviour results from a combination of both the lower hydrogen content in the envelope, and the enhanced CNO efficiency in the H-burning shell, that both concur to burn the hydrogen-rich envelope much faster than in stars of the same mass but lower metallicity and helium content.

The recent past: extended AGB tracks. The insufficient extension of the classical models for AGB stars has been cured by the new models calculated over the past decade, thanks in particular to the adoption of opacities for the model envelopes, that increase significantly when passing from oxygen- to carbon-dominated abundances (Marigo 2002; Marigo & Girardi 2007; Marigo et al. 2008; Weiss & Ferguson 2009). The Padua and BaSTI stellar model libraries have included the TP-AGB phase according to the prescriptions by Marigo et al. (2008) and Cordier et al. (2007), using *synthetic AGB-models* (Iben & Truran 1978; Renzini & Voli 1981; Groenewegen & de Jong 1993; Marigo, Bressan & Chiosi 1996), as described above. Synthetic models are in turn calibrated against the full stellar models and observational data.

This study. Despite the more extended AGB phase brought by the improved opacities (Marigo 2002), the refined prescriptions for synthetic models adopted by Marigo et al. (2008), and new sets of stellar models and isochrones presented by Bertelli et al. (2007, 2008, 2009) and Nasi et al. (2008), there are some properties of the classical *Padua Library* (Bertelli et al. 1994, - <http://pleiadi.pd.astro.it/>) that went lost in the subsequent releases. First of all, the large range of metallicities and initial masses (including massive stars), and the Hot-HB and AGB-manqué evolutionary channels, plus others not relevant to this discussion. As the Bertelli et al. (1994) isochrones have been widely used to study spectro-photometric properties of a large variety of astrophysical objects, from star clusters to galaxies of different morphological types (see Bertelli et al. 1994, and the many papers referring to it) both in the nearby and high redshift Universe, instead of generating new isochrones and SSPs based entirely on the new stellar models by Weiss & Ferguson (2009) – that cover a much smaller range of initial masses and chemical compositions (see below) – we consider the Bertelli et al. (1994) isochrones until the E-AGB phase, and add the TP-AGB models of Weiss & Ferguson (2009). Important similarities between these two model sets ensure that the match can be performed safely. The new AGB models by Weiss & Ferguson (2009) allows us to discriminate between carbon-rich and oxygen-rich stages of the AGB evolution of stars of different mass and initial chemical composition. This improves upon the previous SSP models with dust

by Piovan, Tantalò & Chiosi (2003), that could not follow the evolution of the C and O surface abundances of the AGB stars, and the oxygen- to carbon-rich envelopes was roughly estimated from the old synthetic AGB models by Marigo & Girardi (2001). Updating SSP and SED calculation in presence of dust was not possible for long time, because the synthetic AGB models with variable opacities in outer envelopes and a more realistic description of oxygen- and carbon-rich regimes by Marigo et al. (2008, and references) were not public.

The main characteristics of our adopted model libraries can be summarized as follows:

(i) The stellar models of the Bertelli et al. (1994) library are those of Alongi et al. (1993), Bressan et al. (1993), Fagotto et al. (1994a,b,c), Girardi et al. (1996) and were calculated with the Padua stellar evolution code. All evolutionary phases, from the zero age main sequence to the start of the TP-AGB stage or central C-ignition are included, as appropriate for the mass of the model. We have considered the metallicities $Z=0.0001$, 0.0004 , 0.004 , 0.008 , 0.02 , and 0.05 . The case with $Z=0.1$ is not included (see below). For all models, the primordial He-content is $Y=0.23$ and the He enrichment law is $\Delta Y/\Delta Z=2.5$.

(ii) The stellar models of Weiss & Ferguson (2009) have initial masses in the range from 1 to $6 M_{\odot}$ and metallicities from $Z=0.004$ to $Z=0.05$; they cannot be used to calculate both very young and very old isochrones and neither deal with very low and/or very high metallicities. The models of Weiss & Ferguson (2009) were calculated with the GARSTEC code (see Weiss & Schlattl 2008, for a description of the code).

(iii) The very high metallicity $Z=0.1$ cannot be included because Weiss & Ferguson (2009) new AGB models are not available with this composition. Although the very high metallicity stars may appear as Hot-HB and even AGB manqué objects, (models predict that at $Z=0.1$ this should occur for ages above ~ 8.5 Gyr), still a large number of objects is expected to evolve through the standard AGB phase and develop a thick dust-rich envelope. Neglecting the presence of stars of very high Z – albeit in small percentages – could affect comparisons of models with the MIR-FIR emission of stellar populations in the nuclear regions of giant elliptical galaxies (Bressan, Chiosi & Fagotto 1994). We have a similar problem also at the very low metallicity $Z=0.0001$. The lowest metallicity in the AGB models by Weiss & Ferguson (2009) is $Z=0.0004$. The problem is here less severe, and can be easily cured by extrapolating the properties of the $Z=0.0004$ AGB models, down to $Z=0.0001$.

(iv) Finally, both groups of models make use of the Grevesse & Noels (1993) solar metal mixture.

3 THE GARSTEC AGB MODELS

This section describes briefly the key aspects of the AGB phase, and summarizes Weiss & Ferguson (2009) model prescriptions for mass and opacities. Our new libraries of SEDs for dust-enshrouded AGB stars are based on these stellar models and make use of the same mass-loss rates

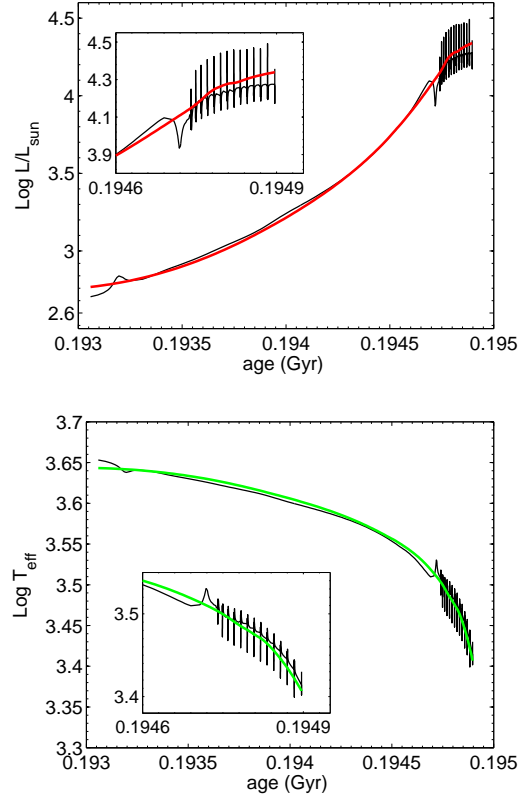


Figure 1. Evolutionary track for the AGB phase of a $M=4 M_{\odot}$, $Z=0.02$ stellar model. The top panel shows the temporal variation of the luminosity, the bottom panel the evolution of the effective temperature. We display, superimposed on the track, the smooth approximations we have adopted.

and the same opacities.

AGB stars in a nutshell. AGB stars are found in the high luminosity and low-temperature region of the HRD. They have evolved through core H- and He-burning, to develop an electron degenerate CO-core. The luminosity is produced by alternate H-shell and He-shell burnings during the TP-AGB phase (see the classical review Iben & Renzini 1983). In brief, the He-burning shell becomes thermally unstable (mild He-burning flash) every $\approx 10^5$ yrs, depending on the core mass. The energy provided by the thermal pulse drives the He-burning convective zone inside the He-rich inter-shell region, and He nucleosynthesis products are mixed inside this region. The stars expand and the H-shell is pushed to cooler regions, where it is almost extinguished. At this stage the lower boundary of the convective envelope can move inwards (in mass) to regions previously mixed by the flash-driven convective zone. This phenomenon is known as third dredge-up (TDU) and is the responsible for enriching the surface with ^{12}C and other products of He-burning. Following the TDU, the star contracts and the H-shell is re-ignited, providing most of the surface luminosity for the next inter-pulse period. This cycle *inter-pulse-thermal pulse-dredge-up* can occur many times during the AGB phase, depending on the initial stellar mass, composition, and in particular on the mass-loss rate. In intermediate-mass AGB stars (M

$\gtrsim 4M_{\odot}$) the convective envelope can dip into the top of the H-shell when it is active, and nuclear H-burning can occur at the base of the convective envelope. This event is called *envelope burning* (EB) or hot bottom burning, and can dramatically change the surface composition. Indeed, the convective turn-over time of the envelope is ≈ 1 year, hence the whole envelope will be processed in a few thousand times over one inter-pulse period. As a consequence, an AGB star of suitable mass can evolve from an oxygen-rich giant to a carbon-rich star ($[C/O] \geq 1$) due to the third dredge-up, and back to an oxygen-rich surface composition, due to CN-burning in the envelope. The new AGB models by Weiss & Ferguson (2009) include the latest physical inputs as far as the treatment of C-enrichment of the envelope due to the TDU and related opacities are concerned. These latter determine the surface temperature of the models and the dust-driven mass-loss rates, in turn affecting the transition to the post AGB stages (Marigo 2002).

3.1 Mass-Loss and Opacities

Mass-Loss. The AGB evolution is characterized by strong mass-loss due to stellar winds. Mass-loss is one of the driving mechanisms of AGB evolution as it determines how and when the TP-AGB phase ends, and what yields can be expected from these stars. It will also affect the nuclear burning at the bottom of the convective envelope. The mass-loss rate for the RGB and pre-AGB evolution is the Reimers (1975) relation,

$$\dot{M} = 4 \times 10^{-13} \frac{(L/L_{\odot})(R/R_{\odot})}{(M/M_{\odot})} \eta_R \quad (1)$$

with $\eta_R = 0.45$. The rate is in M_{\odot}/yr . This is consistent with the mass-loss rate adopted by Bertelli et al. (1994, and companion papers). If and when, along the TP-AGB and later stages, observed mass-loss rates are higher than predicted by Eq. (1), the following prescription is adopted: for carbon-rich chemical compositions (in which nearly all oxygen is bound in CO, and the excess carbon gives rise to carbon-based molecules and dust) the mass-loss rate by Wachter et al. (2002) is used

$$\dot{M}_{\text{AGB}} = 3.98 \times 10^{-15} \left(\frac{L}{L_{\odot}} \right)^{2.47} \left(\frac{T_{\text{eff}}}{2600\text{K}} \right)^{-6.81} \left(\frac{M}{M_{\odot}} \right)^{-1.95} \quad (2)$$

whereas for oxygen-rich stars ($[C/O] < 1$), the empirical fitting formula by van Loon et al. (2005), obtained from dust-enshrouded oxygen-rich AGB stars, is considered.

$$\dot{M}_{\text{AGB}} = 1.38 \times 10^{-10} \left(\frac{L}{L_{\odot}} \right)^{1.05} \left(\frac{T_{\text{eff}}}{3500\text{K}} \right)^{-6.3} \quad (3)$$

As a star leaves the AGB, its T_{eff} increases; by using hydro-simulations of dusty envelopes around evolving post-AGB stars, Schönberner & Steffen (2007) show that strong mass-loss should occur for temperatures higher than $T_{\text{eff}} \simeq 5000\text{ K}$ or $\simeq 6000\text{ K}$. This trend is reproduced by keeping the AGB-wind mass-loss rates until the pulsation period P has dropped to 150 days. As the beginning of the post AGB phase is usually taken at $P = 100$ days, an interpolation is needed to connect the end of the AGB and the start of the post AGB phases. From there on, Weiss & Ferguson (2009) employ the larger rate of either Eq. (1) or the radiation-

driven wind mass loss rate (M_{\odot}/yr):

$$\dot{M}_{\text{CSFN}} = -1.29 \times 10^{-15} \left(\frac{L}{L_{\odot}} \right)^{1.86}. \quad (4)$$

Opacities. The C-enhancement of the stellar envelopes due to the TDU, is treated by using opacity tables with varying $[C/O]$ -ratio, and theoretical mass-loss rates for carbon stars. More precisely, OPAL tables for atomic Rosseland opacities by Iglesias & Rogers (1996) were obtained from the OPAL-website², whereas for low temperatures new tables with molecular opacities were generated following the prescriptions by Ferguson et al. (2005). In all cases, the chemical compositions of low- and high-temperature tables are the same, and tables from the different sources are combined (Weiss & Schlattl 2008). The spectra of M-, S- and C-type giant stars show the presence of different types of molecules, whose abundances are regulated by the $[C/O]$ -ratio. The spectra of O-rich stars ($[C/O]$ -ratio $\lesssim 1$) show strong bands of TiO, VO, H₂O, whereas C-rich stars with $[C/O] > 1$ display C₂, CN, SiC, some HCN, and C₂H₂ bands. Different tabulations of Rosseland opacities at low temperature must be prepared in advance at varying the $[C/O]$ -ratio, for different combinations of X, Y, and Z. The dependence of the opacity on the $[C/O]$ -ratio at given total metallicity cannot be easily foreseen.

3.2 Smoothing the AGB phase

Although the TP-AGB phase is characterized by periodic oscillations (a manifestation of the thermal pulses) of the luminosity and effective temperature of the star, there is a steady increase of the mean luminosity and a decrease of the mean effective temperature. The typical trend of the two quantities is shown in Fig. 1 for a $4M_{\odot}$ star with $Z=0.02$. The inclusion of this oscillatory phase in isochrones and SSPs would be a cumbersome affair from a numerical point of view, with no real advantage compared to adopting the mean luminosity and effective temperature, simply because the oscillations take place on a very short time scale (essentially, the inter-pulse time scale of the thermally pulsing He-burning shell in the deep interior of the star). Therefore, the standard procedure for including the AGB phase envisages a smoothing of the luminosity/effective temperature evolution, and makes use of the resulting mean values (Bertelli et al. 1994; Girardi et al. 2002; Bertelli et al. 2008). To appreciate the reasons for this approximation, some additional comments are necessary:

- In principle it is possible, but in practice it is numerically very cumbersome, to interpolate between the oscillating $L/L_{\odot} - T_{\text{eff}}$ paths of stars of different mass. Since the AGB phase is short-lived, the interpolation between pulses would require short age-differences, corresponding to almost infinitesimal mass differences along an isochrone.

- Star clusters have a small number of AGB stars, as expected according to the short duration of the double shell H-He nuclear burning phase. Therefore, both colour-colour

² <http://physci.llnl.gov/Research/OPAL>

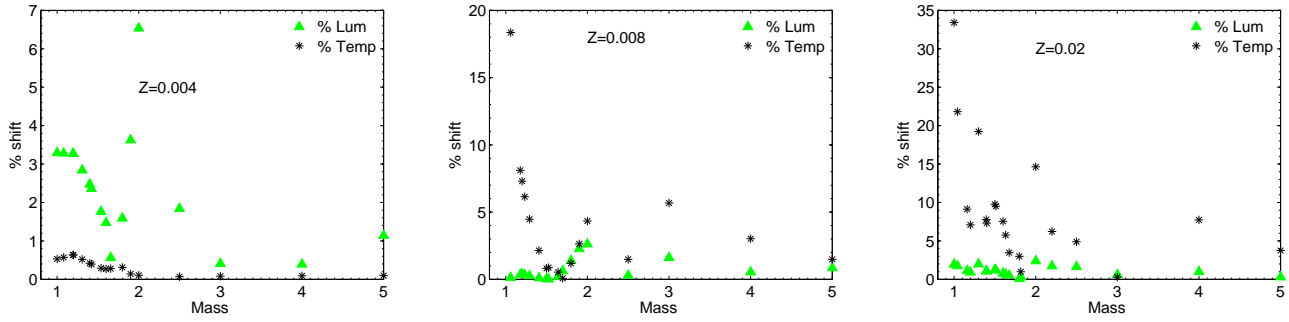


Figure 2. Relative variation $\Delta f/f$ of effective temperature (black stars) and luminosity (green triangles) as a function of the initial stellar mass, between the Bertelli et al. (1994) and Weiss & Ferguson (2009) tracks at the end of the E-AGB phase. Results for three metallicities are displayed: $Z \simeq Z_{\text{SMC}}=0.004$, $Z \simeq Z_{\text{LMC}}=0.008$ (typical of LMC) and $Z \simeq Z_{\text{SN}}=0.02$ (Solar Neighbourhood).

diagrams and CMDs of real clusters cannot reveal photometric signatures of the pulses. In case of very rich assemblies of stars – like field objects in a galaxy – that sample rich populations of AGB stars, one could in principle detect signatures of the oscillations associated to the thermal pulses, if all objects were of the same mass. In practice, AGB stars in a galaxy span a large range of masses, and their paths on the CMD would overlap, to produce a stream of AGB stars of different mass (and probably chemical composition as well) at different stages of their AGB evolution.

Based on these considerations, the thermal pulses have been replaced by smoothed quantities in all evolutionary sequences that include the AGB phase. The procedure can be summarized as follows:

- i) For each evolutionary sequence of fixed mass (and chemical composition) that includes the AGB phase, we have determined the start, duration and end of all the evolutionary phases of interest, to carefully select the TP-AGB stage;
- ii) As discussed in Weiss & Ferguson (2009), nearly all evolutionary sequences under consideration are followed to the end of the AGB phase, but for the highest masses (typically 5 and 6 M_{\odot}), because of numerical difficulties. In such cases, considering the rate of mass-loss and the mass of the remaining envelope of the last model, an estimate of the number of missing pulses until the end of the TP-AGB is provided by Weiss & Ferguson (2009). We use this estimate to evaluate correctly the total TP-AGB lifetime for the few evolutionary sequences where this is required.

iii) Using the MATLAB environment, we plot for each star the current mass (M/M_{\odot}), age (yr), mass-loss rate \dot{M} , luminosity $\log(L/L_{\odot})$, effective temperature $\log T_{\text{eff}}$, gravity $\log g$, central hydrogen mass fraction X_c and central helium Y_c , the core mass within the H- and He-burning shells, M_{c1} and M_{c2} , and the surface abundances of C_s and O_s , both as function of the age and/or mass as appropriate. Making use of *cftool* (*Curve Fitting Toolbox*) and *Smooth Options Loess* (Locally weighted scatter plot smoothing) we try to reproduce each of the above quantities by means of analytical fits. The method uses linear least-squares fit and second-order polynomials. The span parameter, that is the number of data points used to compute each smoothed value, is suitably varied. In locally weighted smoothing methods like *Loess*, if the span parameter is less than 1, it can be

interpreted as the percentage of the total number of data points. For all the physical variables that do not oscillate, smoothing is not required and the span can be varied in such a way that the shape and the form of the original data are preserved¹

iv) Once the smoothing procedure has been applied, we determine the start and the end of the E-AGB and TP-AGB phases, and the oxygen-rich to carbon-rich transition. This is required for the interpolation between different values of the initial mass, to account correctly for the carbon-rich and oxygen-rich stages.

v) In order to include these new models of AGB stars in old isochrones and SSPs, we need to extend Weiss & Ferguson (2009) evolutionary models to mass as low as 0.6 M_{\odot} (at least). As already recalled, Weiss & Ferguson (2009) data set extend only down to 1 M_{\odot} . To this aim, we gently extrapolate the Weiss & Ferguson (2009) stellar models down to 0.8 M_{\odot} trying to scale consistently all the physical variables (luminosity, T_{eff} , time-scales) obtained for 1 M_{\odot} . We follow a numerical technique similar to the one used for the smoothing procedure. For even lower masses, that never reach the carbon-rich phase, a simple description is sufficient, and we follow Bertelli et al. (1994) and Piovan, Tantalo & Chiosi (2003).

vi) Finally, we match the TP-AGB part of each sequence derived from the Weiss & Ferguson (2009) models to the end of the E-AGB phase of the corresponding (same initial mass and chemical composition) evolutionary tracks from Bertelli et al. (1994). Some details of this are given below.

3.3 Matching GARSTEC to Padua models

Both GARSTEC and Padua models, beside the same assumptions for the mass-loss rates until to the start of TP-AGB phase, similar sources and treatment of the opacities, same metal mixture (Grevesse & Noels 1993), and many other common physical ingredients, are calculated with numerical codes that are descendants of the Göttingen code developed by Hofmeister, Kippenhahn & Weigert (1964). This makes easier the match between evolutionary models from the main sequence to the E-AGB phase calculated by

¹ See <http://www.mathworks.it/help/techdoc/index.html> for the MATLAB documentation and more details.

Table 1. Fraction of a SSP total stellar mass at birth, contained in several stellar mass ranges (see text for the definitions) as prescribed by several IMFs. The normalization constants are set to one. Column (1) lists the chosen IMF; (2) & (3) the corresponding lower and upper mass integration limits; (4) fraction contained in stars with mass larger than $1M_{\odot}$; (5): fraction contained in stars with $M < 1M_{\odot}$, which do not contribute to the chemical enrichment; (6) & (7) fraction contained in stars that contribute to the star-dust budget via the AGB and SN channel; (8) the total SSP mass M_{SSP} at birth, in solar units.

IMF		M_l	M_u	$\zeta_{>1}$	$\zeta_{<1}$	$\zeta_{1,6}$	$\zeta_{>6}$	M_{SSP}
(1)		(2)	(3)	(4)	(5)	(6)	(7)	(8)
Salpeter	IMF _{Salp}	0.10	100	0.392	0.6075	0.2285	0.1640	5.826
Larson Solar Neighbourhood	IMF _{Lar-SN}	0.01	100	0.439	0.5614	0.3130	0.1256	2.306
Larson (Milky Way Disc)	IMF _{Lar-MW}	0.01	100	0.653	0.3470	0.3568	0.2962	3.154
Kennicutt	IMF _{Kenn}	0.10	100	0.590	0.4094	0.3883	0.2023	3.048
Kroupa (original)	IMF _{Kro-Ori}	0.10	100	0.405	0.5948	0.3016	0.1036	3.385
Chabrier	IMF _{Cha}	0.01	100	0.545	0.4550	0.3517	0.1933	0.025
Arimoto	IMF _{Ari}	0.01	100	0.500	0.5000	0.1945	0.3055	9.210
Kroupa 2002-2007	IMF _{Kro-27}	0.01	100	0.380	0.6198	0.2830	0.0972	3.134
Scalo	IMF _{Sca}	0.10	100	0.320	0.6802	0.2339	0.0859	4.977

the Padua group, and those for the TP-AGB phase calculated by Weiss & Ferguson (2009).

We carefully checked that, with some exceptions, the shifts we must apply to Weiss & Ferguson (2009) TP-AGB models to match the Bertelli et al. (1994) E-AGB endpoints are acceptable. We have scaled luminosity, effective temperature, core mass, and envelope mass of the GARSTEC tracks to match those of the E-AGB stage of Bertelli et al. (1994) models. The zero point of the age of GARSTEC AGB models is also rescaled to match that of Bertelli et al. (1994) E-AGB endpoint. Figure 2 displays the required $\log T_{\text{eff}}$ and $\log(L/L_{\odot})$ shifts, for the initial masses under consideration. Recalling that the luminosity of stellar models is far less affected by theoretical uncertainties than the effective temperature, we analyze the match of the two sets of tracks by means of the relative variations of luminosity and effective temperature, defined in the following way: let L_f and $T_{\text{eff},f}$ be the luminosity/effective temperature of the final model of the E-AGB phase and L_i and $T_{\text{eff},i}$ the counterparts for the initial model of the TP-AGB phase, the relative luminosity shift is given by

$$\Delta f/f = |\log(L_i/L_{\odot}) - \log(L_f/L_{\odot})| / \log(L_i/L_{\odot}).$$

For the effective temperature it is more convenient to normalize the shift to the total length of the TP-AGB phase projected onto the T_{eff} -axis, i.e.

$$\Delta f/f = |\log T_{\text{eff},i} - \log T_{\text{eff},f}| / (\log T_{\text{eff},1} - \log T_{\text{eff},i}),$$

where $T_{\text{eff},1}$ is the temperature of the last TP-AGB point. Figure 2 displays results for three values of the metallicity, namely $Z=0.004$ (typical of the SMC), $Z=0.008$ (typical of the LMC), and $Z=0.02$ (approximately solar). Models for other metallicities behave in the same way. For low-mass stars, whose lifetime on the TP-AGB is very short, shifts comparable to the total temperature interval of the TP-AGB phase are possible. This is evident in Fig. 2: the low-mass, high-metallicity models need the largest shifts in temperature. This is due to the strong sensitivity of the envelope size (hence effective temperature) to the mean opacity and to the amount of mass lost in the previous phases – see Eq. (1) – which governs the mass-loss during the RGB and pre-AGB evolution. Indeed, even though GARSTEC and Padua models include very similar recipes for the mass-loss

and the opacities, the evolutionary time spent in the pre-AGB phases may still vary because of other different input physics of the models like, e.g., nuclear reaction rates, thus causing a different size of the envelope. The luminosity is much more stable because it is generated deep inside the star. For the other mass ranges and metallicities involved in the TP-AGB, the shifts are $\lesssim 5\%$, thus introducing an unavoidable, but small, uncertainty in the region of the HR diagram covered by TP-AGB stars. In particular, for the highest masses, the shifts are just a small fraction of the full TP-AGB extension.

3.4 The Initial Mass Function

To calculate spectro-photometric properties of SSPs (SED, magnitudes, colours and luminosity functions) it is necessary to consider an IMF. There are several popular prescriptions in the literature. A few of them are listed in Table 1. For the purposes of our study all IMFs are assumed to be constant in time and space. The IMFs in our list are: Salpeter (Salpeter 1955, IMF_{Sal}), Larson (Larson 1998, IMF_{Lar-MW}, IMF_{Lar-SN}), – with different parameters for the Milky Way disk and for the solar neighbourhood (Portinari, Sommer-Larsen & Tantalo 2004) – Kennicutt (Kennicutt 1998, IMF_{Kenn}), the original IMF by Kroupa (Kroupa 1998, IMF_{Kro-Ori}), a revised and more recent version of this IMF by Kroupa (Kroupa 2007, IMF_{Krou-27}), Chabrier (Chabrier 2003, IMF_{Cha}), Scalo (Scalo 1986, IMF_{Sca}), and Arimoto & Yoshii (Arimoto & Yoshii 1987, IMF_{Ari}). We refer either to the original sources or to Piovan et al. (2011) for a detailed explanation of the main features of these IMFs.

The IMFs are expressed as the number of stars per mass interval, $dN = \Phi(M)dM$, and require a normalization, for $\Phi(M)$ contains an arbitrary constant. This can be accomplished in different ways. In view of the calculation of integrated spectral energy distributions, magnitudes and colours of the SSPs, we introduce here the concept of (zero age) SSP mass, given by

$$M_{SSP} = \int_{M_l}^{M_u} \Phi(M) M dM \quad (5)$$

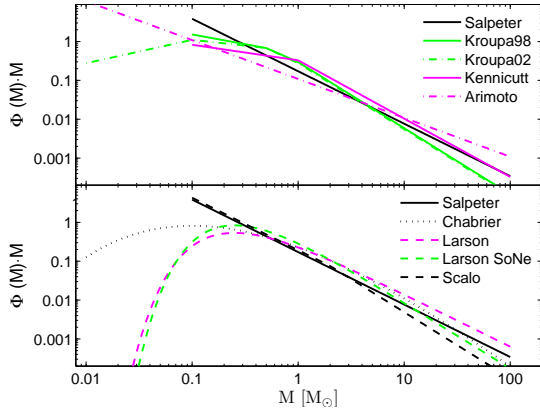


Figure 3. Fractional contribution to the total SSP mass budget of stars of different masses, as predicted by the labelled IMFs over the range where they are defined (see text for details). The widely used IMF by Salpeter (1955) is shown in both panels for the sake of comparison. Stellar masses are in solar units and all the IMFs are in this case normalized to a total SSP mass equal to $1M_{\odot}$.

i.e. the total mass contained in a SSP with lower stellar mass limit M_l and upper mass limit M_u , and we set the constant entering $\Phi(M)$ equal to one. The photometric properties of a SSP of given age and chemical composition will refer to a given SSP mass. By doing this, one can easily scale the SSP monochromatic flux to any population of stars of arbitrary total mass.

For the purposes of the discussion below, we denote with ζ_1 the the fraction of the population total stellar mass at birth, contained in stars whose lifetime is shorter than the age of the Universe, – and therefore able to chemically pollute the interstellar medium – given by

$$\zeta_1 = \frac{\int_{M_l}^{M_u} \Phi(M) M dM}{\int_{M_l}^{M_u} \Phi(M) M dM} \quad (6)$$

where M_l and M_u have the same meaning as before. In a similar way, we define the mass fraction of the stars contributing to the dust-budget via the AGB channel ($1M_{\odot} \leq M \leq 6M_{\odot}$) denoted by $\zeta_{1,6}$, and the mass fraction of stars that contribute to the dust budget via the core collapse supernovae channel, ($M > 6M_{\odot}$) denoted by $\zeta_{>6}$. Table 1 summarize the mass ranges where the various IMFs are defined, the mass fractions of stars defined above, and the corresponding total SSP mass at birth, for a normalization constant equal to one.

Figure 3 shows the mass dependence of the different IMFs, and implicitly the mass interval covered by stars going through the TP-AGB and WD phases or ending in a SN explosion and thus contributing to the star-dust budget.

4 THE NEW ISOCHRONES: RESULTS

We present here the sets of isochrones obtained with the new TP-AGB models. Each set contains isochrones for more than fifty age values, ranging from ~ 3.0 Myr to 15 Gyr. The age range for the development of an AGB varies with metallicity according to

- $Z=0.050$: $7.78 \leq \log t \leq 10.18$;
- $Z=0.020$: $7.90 \leq \log t \leq 10.18$;
- $Z=0.008$: $8.10 \leq \log t \leq 10.18$;
- $Z=0.004$: $8.10 \leq \log t \leq 10.18$;
- $Z=0.0004$: $8.10 \leq \log t \leq 10.18$;
- $Z=0.0001$: $8.00 \leq \log t \leq 10.18$.

where t is in yr. All the isochrones are calculated with the IMF_{Salp}: indeed, varying the IMF would affect only the way the different mass bins along an isochrone are populated, i.e. the so-called normalized luminosity function. The effect of changing the IMF becomes more evident when calculating SEDs of SSPs (see below).

Figure 4 shows a few selected isochrones for metallicities $Z=0.004$ (typical for the SMC), $Z=0.02$ (typical for the LMC), and $Z=0.02$ (typical for the Sun and the solar vicinity) respectively. All other metallicities have similar HRDs. Important differences with Bertelli et al. (1994) arise obviously along the AGB phase, as shown in Fig. 5. The AGB phase for oxygen-rich envelopes is displayed with black, solid lines, whereas the carbon-rich case with $[C/O]>1$ is displayed with magenta dot-dashed lines. The beginning and end of each evolutionary phase is marked with a little star. Thanks to the new low temperature opacities (Weiss & Ferguson 2009), the isochrones now extend towards lower temperatures than in the old models. The enrichment of the C-abundance at the surface of TP-AGB stars, accompanied by an important reduction of the effective temperature and the formation of a shell of dust surrounding the star (see below) are important steps forward, that amply justify our efforts to calculate a library of stellar spectra for O- and C-rich dust-enshrouded AGB stars.

Looking at the grids of isochrones for different metallicities, the following considerations can be made:

-**Solar and super-solar metallicities:** $Z \geq 0.02$. These stars are normally oxygen-rich at the surface, even if a late transition to the carbon-rich phase may take place due to the final dredge-up events, in agreement with observations (e.g. see van Loon et al. 1998, 1999, for more details). For solar metallicity, the transition occurs only in isochrones of intermediate ages and at very low T_{eff} , during the final stages of the TP-AGB phase. In contrast, isochrones of super-solar metallicity show only oxygen-rich material at the surface. As expected, the youngest isochrones are the most extended in the HRD during the AGB phase. The TDU does not occur in the oldest isochrones of both metallicities, and the TP-AGB phase is much shorter than the E-AGB phase.

-**Sub-solar metallicities:** $0.004 \leq Z < 0.02$. These stars show an extended carbon-rich phase, even at rather young ages. This is due to the onset of the ON cycle, that converts O into N, increasing the $[C/O]$ -ratio above 1 (Ventura, D’Antona & Mazzitelli 2002; Marigo et al. 2008). Furthermore, the carbon-enrichment at the surface starts at higher effective temperatures (compared to solar metallicity isochrones), because the lower molecular concentrations in the atmospheres (Marigo et al. 2008).

-**Low metallicities:** $Z < 0.004$. All trends described for isochrones of moderate metallicities become more evident. The transition to a carbon-rich envelope starts at even higher effective temperatures and the majority of the isochrones show almost exclusively the C-star phase. Only few isochrones of intermediate ages have an oxygen-rich

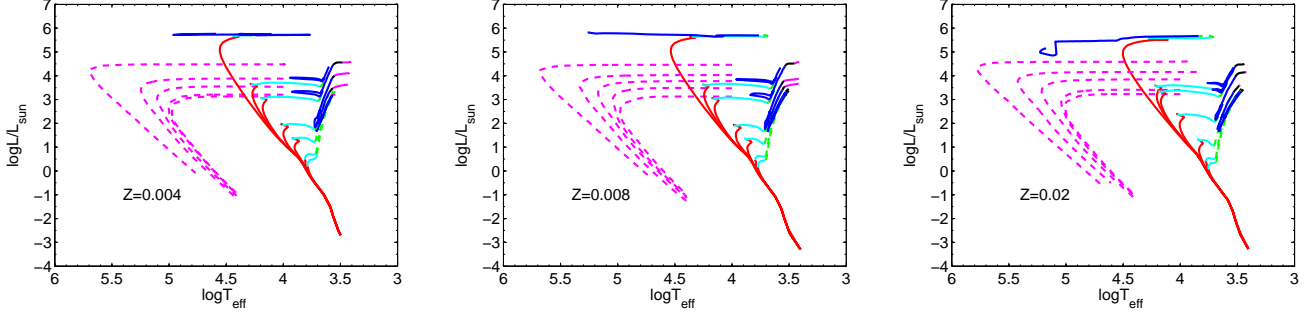


Figure 4. Isochrones with the new AGB models, from the zero age main sequence to the stage of PN formation or central carbon ignition, depending on the initial stellar mass. Three metallicities are shown: $Z=0.004$, typical of the Small Magellanic Cloud (left), $Z=0.008$, typical of the Large Magellanic Cloud (middle), and $Z=0.02$, typical of the Solar neighbourhood (right). The isochrones are plotted for a few selected ages between 5 Myr and 15 Gyr.

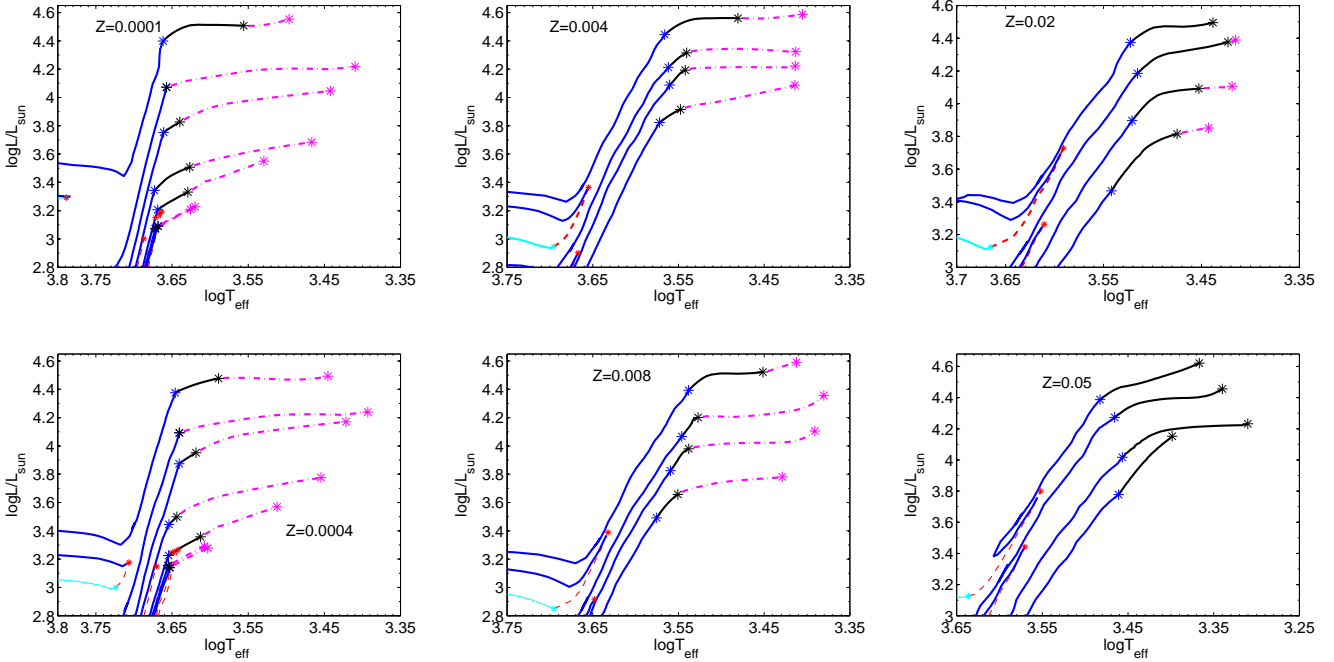


Figure 5. Isochrones in the theoretical HRD, centred on the E-AGB and TP-AGB phases, for the labelled metallicities. They are organized in three groups, from left to right. **Left Panels:** Very low metallicities, $Z=0.0001$ and $Z=0.0004$ respectively. **Central Panels:** as in the left panels, but for $Z=0.004$ and $Z=0.008$. **Right Panels:** as in the previous panels, but for $Z=0.02$ (solar value) and $Z=0.05$. Along each isochrone the end of the E-AGB phase is marked by the blue star. The TP-AGB phase is in turn drawn as a solid black line when the envelope is oxygen-rich, and as a dot-dashed magenta line when it is carbon-rich.

phase. Our results fairly agree with those by Marigo et al. (2008) even though some marginal differences can be noticed. The agreement is ultimately due to the fact that both include opacities that depend on the $[C/O]$ -ratio. This is confirmed by the nearly identical effective temperatures of the AGB models, and the similar behaviour of the oxygen-rich and carbon-rich stages with the metallicity.

5 THE DUST-FREE SSPS

The most elementary population of stars is the so-called *Single* (or *Simple*) *Stellar Population* made of stars born at the

same time in a burst of star formation activity of negligible duration, and with the same chemical composition. SSPs are the basic tool to understand the spectro-photometric properties of more complex systems like galaxies, which can be considered as linear combinations of SSPs with different composition and age, each of them weighted by the corresponding rate of star formation.

The integrated monochromatic flux $ssp_{\lambda}(\tau, Z)$ of a SSP of any age and metallicity is given by

$$ssp_{\lambda}(\tau, Z) = \int_{M_l}^{M_u} \Phi(M) f_{\lambda}(M, \tau, Z) dM \quad (7)$$

where f_λ is the monochromatic flux of a star of mass M , metallicity Z and age τ . $\Phi(M)$ is the IMF, expressed as the number of stars per mass interval dM . The integrated $ssp_\lambda(\tau, Z)$ refers to an ideal SSP of total mass M_{SSP} (expressed in solar units). The integrated bolometric luminosity is then calculated by integrating $ssp_\lambda(\tau, Z)$ over the whole wavelength range:

$$L_{\text{SSP}}(\tau, Z) = \int_0^\infty ssp_\lambda(\tau, Z) d\lambda \quad (8)$$

In more detail, the steps to calculate the SED of a SSP are as follows:

(i) for a fixed age and metallicity, the corresponding isochrone in the HRD is divided into elementary intervals small enough to ensure that luminosity, gravity, and T_{eff} are nearly constant. In practice, the isochrone is approximated by a series of virtual stars, to which we assign a spectrum;

(ii) in each interval the stellar mass spans a range ΔM fixed by the evolutionary speed. The number of stars assigned to each interval is proportional to the integral of the IMF over the range ΔM (the differential luminosity function);

(iii) finally, the contribution to the integrated flux (at each wavelength) by each elementary interval is weighted by the number of stars and their luminosity;

(iv) the spectra of the virtual stars are taken from suitable spectral libraries, as a function of effective temperature, gravity, and chemical composition. We employed the spectral library by Lejeune, Cuisinier & Buser (1998), based upon the Kurucz (1995) release of theoretical spectra, with several important implementations. For $T_{\text{eff}} < 3500$ K the spectra of dwarf stars by Allard & Hauschildt (1995) are included, whilst the spectra by Fluks et al. (1994) and Bessell et al. (1989); Bessell, Brett & Scholz (1991) are considered for giant stars. Following Bressan, Chiosi & Fagotto (1994), for $T_{\text{eff}} > 50000$ K the library has been extended using black body spectra.

We have calculated grids of dust-free SSP-SEDs of different ages, for the six values of metallicity, and the nine different IMFs of Tab. 1, and derived magnitudes and colours for different photometric systems.

5.1 A comparison with the old dust-free SSPs

We compare in this section the old SSPs computed by Bertelli et al. (1994) with our new database. The *only improvement* is the TP-AGB phase, based on the new models by Weiss & Ferguson (2009). We start by defining at each wavelength λ a residual flux ratio

$$FR_\lambda = [F_\lambda(\text{Bertelli}) - F_\lambda(\text{Weiss})]/F_\lambda(\text{Weiss}),$$

where $F_\lambda(\text{Bertelli})$ is the monochromatic SSP flux of the SED calculated with the Bertelli et al. (1994) AGB models and $F_\lambda(\text{Weiss})$ is the counterpart with the Weiss & Ferguson (2009) AGB models. The results are presented in Fig. 6, for $Z=0.004$, $Z=0.008$, and $Z=0.02$, respectively. The top panels display the total monochromatic flux for five selected ages, moving from young ages where the AGB phase is well developed, to old ages where the AGB is of much less importance. We define as *cumulative flux* the monochromatic flux integrated between the zero age

main sequence and a given advanced evolutionary phase, like, i.e., the tip of the RGB or the end of the TP-AGB. The bottom panels show, for ages of 3, 5 and 10 Gyr, the cumulative flux to the end of the AGB phase and the total flux, that includes the post-AGB PN and WD phases. There are two regions of the SED where we expect differences, even when dust is not introduced: (1) the near-IR region affected by cool stars and (2) the UV region, because different AGB lifetimes lead to differences in the PN phase. Indeed, Fig. 6 reveals significant differences between old and new SSPs in the UV region (say up to $0.3 \mu\text{m}$). These are likely caused by the different assumptions made by Bertelli et al. (1994) and Weiss & Ferguson (2009) for the mass-loss rate during the TP-AGB phase. The old SSPs make use of the Vassiliadis & Wood (1993) prescription; the new models include the mass-loss rates by either Wachter et al. (2002) or van Loon et al. (2005), depending on the surface chemical compositions of the models. For a given initial mass, different mass-loss rates produce, when the TP-AGB phase is over, remnants with different core masses and, in turn, different PNs. This is clear when looking at the bottom panels of Fig. 6. The cumulative fluxes to the end of the AGB phase do not result in any visible residuals. Instead, the inclusion of the PN phase changes the residuals by as much as 30%. As expected, this effect increases at decreasing ages: higher mass stars experience a larger mass-loss rate and produce remnants (cores) of smaller mass and hotter surface temperatures. Finally, there is a systematic trend of the ratio FR_λ in the UV, when passing from low to high metallicity (see Fig. 6).

Other major differences appear in the IR spectral region, where AGB stars emit most of their light. This is shown by Fig. 7, that displays the ratios FR_λ as a function of age at selected near-IR wavelengths, for different metallicities ($Z=0.004$, 0.008 , and 0.02). Given that we neglect the effects of circumstellar dust shells around the AGB stars, we expect that the cool M and C models emit most of the flux in the range $\sim 1\text{--}4 \mu\text{m}$ (dust would shift the emission towards longer wavelengths). The agreement between the two sets of SSPs is very good before the onset of the AGB phase and for old ages, where the differences amount to only a few per cent. As expected, when the AGB phase sets in at $\log t \sim 8$, differences are much larger. They can be ultimately ascribed to the different prescriptions for the TP-AGB phase in the Padua and GARSTEC models.

6 SSPS WITH CIRCUMSTELLAR DUST AROUND AGB STARS

It has long been known that low and intermediate-mass AGB stars are amongst the main contributors to the ISM dust content. The previous evolutionary phases are not as important as dust factories: dust formation in RGB and E-AGB stars is poorly efficient because of the unfavorable wind properties and the low mass-loss rate (Gail et al. 2009). As for the calculation of SEDs, magnitudes, and colours, the presence of dust shells is usually – with just a few exceptions (see for instance Bressan, Granato & Silva 1998; Mouhcine 2002; Piován, Tantalo & Chiosi 2003; Marigo et al. 2008) – not taken into account.

As TP-AGB stars are expected to form significant

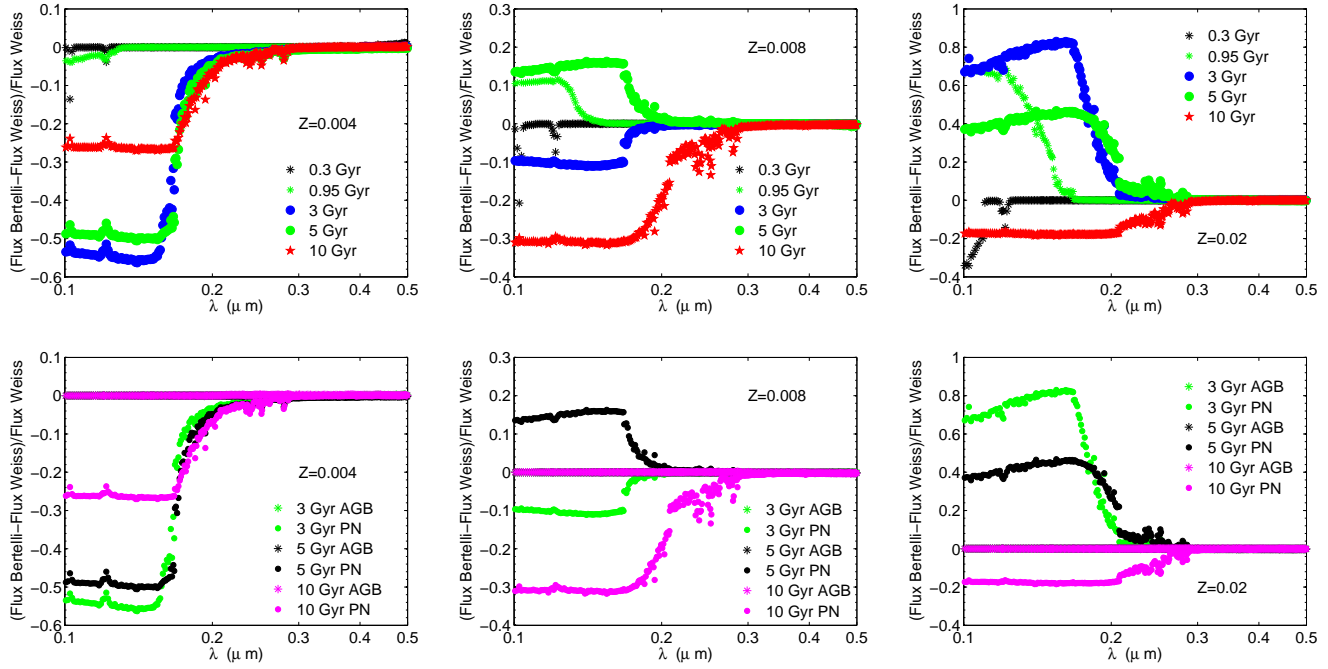


Figure 6. Upper panels: comparison between the integrated flux of our new SSPs and the *old* SSPs, as a function of λ , for the labelled ages and metallicities. Lower panels: as the upper panels, but for both integrated and cumulative fluxes to the end of the AGB, for fewer selected ages. Left panels are for $Z=0.004$, central panels for $Z=0.008$, and right panels for $Z=0.02$.

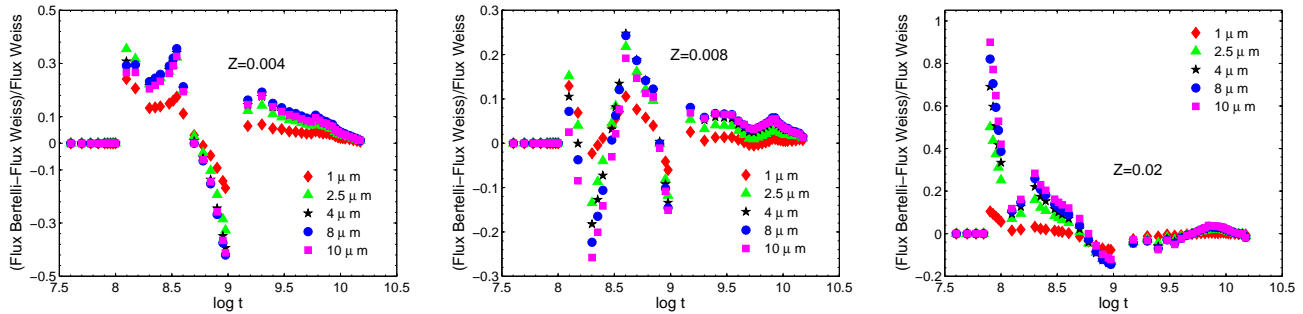


Figure 7. As in the upper panels of Fig. 6, but in this case we consider the residual flux ratios as a function of age for the labelled reference wavelengths λ . Three metallicities are shown: $Z=0.004$ (left panel), $Z=0.008$ (middle panel) and $Z=0.02$ (right panel). The unit of time t is yr.

amounts of dust and therefore suffer self-obscurtion and re-processing of their photospheric radiation, the effect of dust on their SEDs cannot be ignored (Piovan, Tantaló & Chiosi 2003).

Dust formation in AGB stars has been modelled with increased accuracy over the years (Gail, Keller & Sedlmayr 1984; Gail & Sedlmayr 1985, 1987; Dominik, Sedlmayr & Gail 1993; Gail & Sedlmayr 1999; Ferrarotti & Gail 2002, 2006; Gail et al. 2009), and we are now in the position to calculate the amount of newly formed dust in M-stars, S-stars and C-stars (a sequence of growing $[\text{C}/\text{O}]$ -ratio). This ratio determines the composition of dust formed in the outflows (Piovan, Tantaló & Chiosi 2003; Ferrarotti & Gail 2006; Gail et al. 2009). The oxygen-rich M-stars ($[\text{C}/\text{O}] < 1$) produce dust grains mainly formed

by refractory elements (generically named silicates), like pyroxenes and olivines, oxides and iron dust. Carbon-rich stars ($[\text{C}/\text{O}] > 1$) produce carbon-dust; SiC and maybe iron dust can condensate. In S-stars ($[\text{C}/\text{O}] \approx 1$) quartz and iron dust should form (Ferrarotti & Gail 2002). However, the carbon-rich or oxygen-rich phases dominate, and for example the contribution of SiC produced during the S-star phase can be neglected, compared to the SiC produced during the C-star phase.

6.1 Modelling a dusty envelope

The problem of the radiative transfer in the dusty shells that form around AGB stars has been addressed by many authors (see the classical review by Habing 1996, and refer-

ences therein). The best approach would clearly be to couple the equations describing the radiative transfer through the dusty envelope, with the hydro-dynamical equations for the motion of the two components, dust and gas, taking into account the interplay between gas, dust, and radiation pressure. For the purposes of this work, it is however enough to limit ourselves to solve the problem of the radiative transfer through the envelope (Ivezic & Elitzur 1997; Rowan-Robinson 1980). Indeed, our purpose is to build a library of dusty SEDs to determine the effects of dust around AGB stars, not to study the dynamical behaviour of the outflows.

6.1.1 The optical depth

As our aim is to determine the SED of AGB stars after it has been filtered by circumstellar dust shells, we can use DUSTY, the classical code for radiative transfer (Ivezic & Elitzur 1997). The original version of the code cannot handle large wavelength grids without becoming computationally very demanding. To cope with this, we suitably modified the public version 2.06 of DUSTY to handle a much larger grid at still reasonable computational cost. Our full grid is built by adding the Kurucz-Lejeune wavelength grid plus the all the wavelengths characterizing the tabulated optical properties and features of the dust. For the sake of simplicity, we assume spherical symmetry. The key parameter needed to solve the radiative transfer problem is the optical depth τ_λ of the shell, defined as follows:

$$\tau_\lambda = \int_{r_{in}}^{r_{out}} d\tau_\lambda(r) = \int_{r_{in}}^{r_{out}} k_\lambda(r) \rho_d(r) dr \quad (9)$$

where $k_{\lambda,d}$ is the overall dust extinction coefficient per mass unit and ρ_d is the dust mass density. They both depend on the radial distance r from the central source. The integral is evaluated over the thickness of the shell, from the innermost to the outermost radius. If we now apply the continuity equation for the gas and dust (Schutte & Tielens 1989; Piován, Tantaló & Chiosi 2003) we can recast the optical depth of Eq. 9 as

$$\tau_\lambda = \int_{r_{in}}^{r_{out}} k_\lambda(r) \frac{\dot{M}(r) \delta(r)}{4\pi r^2 v_d(r)} dr \quad (10)$$

where δ is the dust-to-gas ratio in the shell. To proceed further, the mass-loss rate $\dot{M}(r)$, the expansion velocity of the dust $v_d(r)$, the extinction coefficient $k_\lambda(r)$, and the dust-to-gas ratio δ together with their radial dependence must be specified. Common assumptions are the following (Groenewegen 1993; Bressan, Granato & Silva 1998; Piován, Tantaló & Chiosi 2003; Groenewegen 2006; Marigo et al. 2008): at any given time, the rate of mass-loss and the velocity are constant and do not depend on r . The same holds for the optical properties of the dust and the dust-to-gas ratio. The radial dependence is neglected. With these simplifications and assuming that $r_{out} \gg r_{in}$ and $r_{in} \sim r_c$ we have

$$\tau_\lambda = \frac{\delta \dot{M} k_\lambda}{4\pi v_\infty r_c} \quad (11)$$

where v_∞ is the wind terminal velocity and r_c the conden-

sation radius or the innermost distance from which dust starts to absorb the stellar radiation. A safe approximation is that $v_d(r) \sim v_\infty$ because of the small drift between gas and dust (Groenewegen 1993). The extinction coefficient per unit mass k_λ is in general given by:

$$k_\lambda = \frac{\sum_i n_i \sigma_i(a, \lambda)}{\rho_d} = \frac{\sum_i n_i \pi a^2 Q_i(a, \lambda)}{\rho_d} \quad (12)$$

where the summation is extended over all types of grains in the envelope, and σ_i and n_i are the cross section and the number of grains per unit volume of the i -th dust type, respectively. For the sake of simplicity only one typical dimension a of the grains is assumed. The total mass density of the grains for unit volume ρ_d , is

$$\rho_d = \frac{4}{3} \pi a^3 \sum_i n_i \rho_i \quad (13)$$

where ρ_i is the mass density of a grain of dust type i , assumed to be spherical. Finally, we get:

$$\tau_\lambda = \frac{3\delta \dot{M}}{16\pi v_\infty r_c} \frac{\sum_i n_i Q_i(a, \lambda)/a}{\sum_i n_i \rho_i} \quad (14)$$

Starting from Eq. 14, introducing a single type of grain and properly normalizing the various quantities, it is possible to recover the expression by Groenewegen (2006) for the optical depth. The inner radius of the shell can be derived from the conservation of the total luminosity $L = 4\pi R_*^2 \sigma T_{\text{eff}}^4 = 4\pi r_c^2 \sigma T_d^4$, thus obtaining

$$\tau_\lambda = A_d \delta \dot{M} v_\infty^{-1} L^{-1/2} \quad (15)$$

where A_d depends on the adopted mixture of dust (Marigo et al. 2008):

$$A_d = \frac{3}{8} T_d^2 \left(\frac{\sigma}{\pi} \right) \frac{\sum_i n_i Q_i(a, \lambda)/a}{\sum_i n_i \rho_i} \quad (16)$$

Different kinds of dust would imply different condensation temperatures T_d , thus leading to different radii r_c . For the sake of simplicity and due to the DUSTY requirements, only a single condensation temperature will be used, even in case of a multi-component dust shell.

We need now to connect the quantities defining the optical depth of the shell with the parameters of the AGB models. We can take the surface bolometric luminosity L/L_\odot , the effective temperature T_{eff} , the mass-loss rate \dot{M} , the metallicity Z , the [C/O]-ratio, and the chemical composition of the star at the surface. To get the terminal velocity of the wind, Bressan, Granato & Silva (1998) and Piován, Tantaló & Chiosi (2003) adopted the simple recipes by Vassiliadis & Wood (1993) and Habing, Tignon & Tielens (1994). In this paper, we employ the formulation of dusty winds by Elitzur & Ivezic (2001) as also done recently by Marigo et al. (2008),

$$v_\infty = \left(A \dot{M}_{-6} \right)^{1/3} \cdot \left(1 + B \frac{\dot{M}_{-6}^{4/3}}{L_4} \right)^{-1/2} \quad (17)$$

where the velocity is in km s^{-1} , the mass-loss rate \dot{M}_{-6} in units of $10^{-6} \text{ M}_{\odot} \text{ yr}^{-1}$, and finally the AGB star luminosity L_4 in units of $10^4 L_{\odot}$. The two parameters A and B are defined as in Elitzur & Ivezić (2001):

$$A = 3.08 \times 10^5 T_{c3}^4 Q_* \sigma_{22}^2 \Psi_0^{-1} \quad (18)$$

$$B = \left(2.28 \frac{Q_*^{1/2} \Psi_0^{1/4}}{Q_V^{3/4} \sigma_{22}^{1/2} T_{c3}} \right)^{-4/3} \quad (19)$$

The meaning of the various parameters contained in the functions A and B is as follows. First, T_{c3} is the dust condensation temperature in units of 10^3 ; literature values range from 800 K to 1500 K (Rowan-Robinson & Harris 1982; David & Papoular 1990; Suh 1999, 2000; Lorenz-Martins & Pompeia 2000; Lorenz-Martins et al. 2001; Suh 2002). Our choice is in the range between 1000 K and 1500 K, depending on the dust mixture and the [C/O]-ratio (see below for more details), in agreement with most of the literature and with similar works on dusty AGBs by Groenewegen (2006) and Marigo et al. (2008). Then, Q_* is the mean of the quantity $Q(\lambda, a)$, averaged over the Planck function $B(\lambda, T_{\text{eff}})$:

$$Q_* = \frac{\pi}{\sigma T_{\text{eff}}^4} \int Q(a, \lambda) B(\lambda, T_{\text{eff}}) d\lambda \quad (20)$$

where $Q(a, \lambda)$ is the sum of the absorption and scattering radiation pressure efficiencies, assuming isotropic scattering. The cross section σ_{22} is defined by the following relation with the gas cross section:

$$\sigma_g = \sigma_{22} \cdot 10^{-22} \text{ cm}^2 \quad (21)$$

where

$$\sigma_g = \pi a^2 \frac{\sum_i n_i}{\sum_i n_{i,g}} = \frac{3}{4} \frac{A_g m_H}{a \bar{\rho}} \delta. \quad (22)$$

Here $n_{i,g}$ is the gas number density, $A_g \simeq 4/(4X_H + X_{He})$ the mean molecular weight of the gas (Marigo et al. 2008), m_H the atomic mass unit and $\bar{\rho}$ the average mass density of the grains calculated for the actual mixture of dust, given by $\bar{\rho} = \sum_i n_i \rho_i / \sum_i n_i$. The parameter Ψ_0 is defined in Elitzur & Ivezić (2001) as:

$$\Psi_0 = \frac{Q_P(T_{\text{eff}})}{Q_P(T_d)} \quad (23)$$

where the subscript P means an average of the absorption efficiency over the Planck function, similar to the average that defines Q_* in Eq. (20). It must be underlined that Elitzur & Ivezić (2001) assume the temperature of the star to be fixed at 2500 K: in our case we will take into account the variation of T_{eff} , by considering every time the temperature of the current stellar model. Finally, the last parameter in Eqs. (18) and (19) is Q_V , the absorption efficiency at optical wavelengths.

6.1.2 Mass-loss

It is currently widely accepted and supported by hydrodynamical calculations, that large amplitude pulsations are required to accelerate the mass outflow from the stellar surface of AGB stars to regions where the gas cools enough so that refractory elements can condense into dust. Once dust grains are formed, they transfer energy and momentum from the stellar radiation field to the gas by collisions, so that the flow velocity may grow enough to exceed the escape velocity (Gilman 1972). This stellar wind increases with time until the so-called super-wind regime is reached: the star quickly evolves into a PN, with the whole envelope being stripped off. The remnant is a bare CO core that evolves to high effective temperatures. We have already reported on the mass-loss rates adopted for the various evolutionary phases from the RGB to the formation of PN stars. They are also used here for the sake of consistency between stellar models and their dusty envelopes. The only point to note is that a minimum mass-loss is required to form enough dust to be able to accelerate the gas beyond the escape velocity (Elitzur & Ivezić 2001). The minimum mass-loss is:

$$\dot{M}_{\text{min}} = 3 \times 10^{-9} \frac{M^2}{Q_* \sigma_{22}^2 L_4 T_{k3}^{1/2}} \quad (24)$$

where T_{k3} is the kinetic temperature at the inner boundary of the shell, that we simply set to $T_{k3} \approx T_{c3}$. It may easily occur that envelopes are optically thin and $\dot{M} \lesssim \dot{M}_{\text{min}}$. In this case dust is formed, but according to Elitzur & Ivezić (2001) it cannot sustain the wind. When this happens, we apply the recipe proposed by Marigo et al. (2008) to evaluate the expansion velocity by means of \dot{M}_{min} , and get an estimate for v_{∞} to insert in the expression for τ_{λ} .

6.1.3 Dust-to-gas ratio

Another important parameter of Eq. (14) is the dust-to-gas ratio δ . In Piovani, Tantaló & Chiosi (2003) the dust-to-gas ratio was obtained by simply inverting a relation between velocity, luminosity and dust-to-gas ratio based upon the results by Habing, Tignon & Tielens (1994).

Over the years, increasingly refined models of AGB stars have simulated the process of dust formation in the envelope (Gail, Keller & Sedlmayr 1984; Gail & Sedlmayr 1985, 1987; Dominik, Sedlmayr & Gail 1993; Gail & Sedlmayr 1999; Ferrarotti & Gail 2001, 2002; Ferrarotti 2003). In Ferrarotti & Gail (2006) dust formation is described through the concept of key species (Kozasa & Hasegawa 1987) and detailed tables of yields of dust for oxygen-rich and carbon-rich stars are presented. The dust grains considered by Ferrarotti & Gail (2006) are pyroxenes, olivines, quartz and iron dust for oxygen-rich M-stars, quartz and iron dust for S-stars, and finally silicon carbide and carbonaceous grains for carbon-rich C-stars. For each one of them, according to the initial metal distribution adopted by Weiss & Ferguson (2009), the key element will be silicon, iron or carbon, depending on the grain type. Indeed, only the abundances of C and O may change during the AGB evolution due to TDU and E-HB, whereas the abundances of Mg, Si, S and Fe remain unchanged. Introducing the key elements and the equations of continuity for

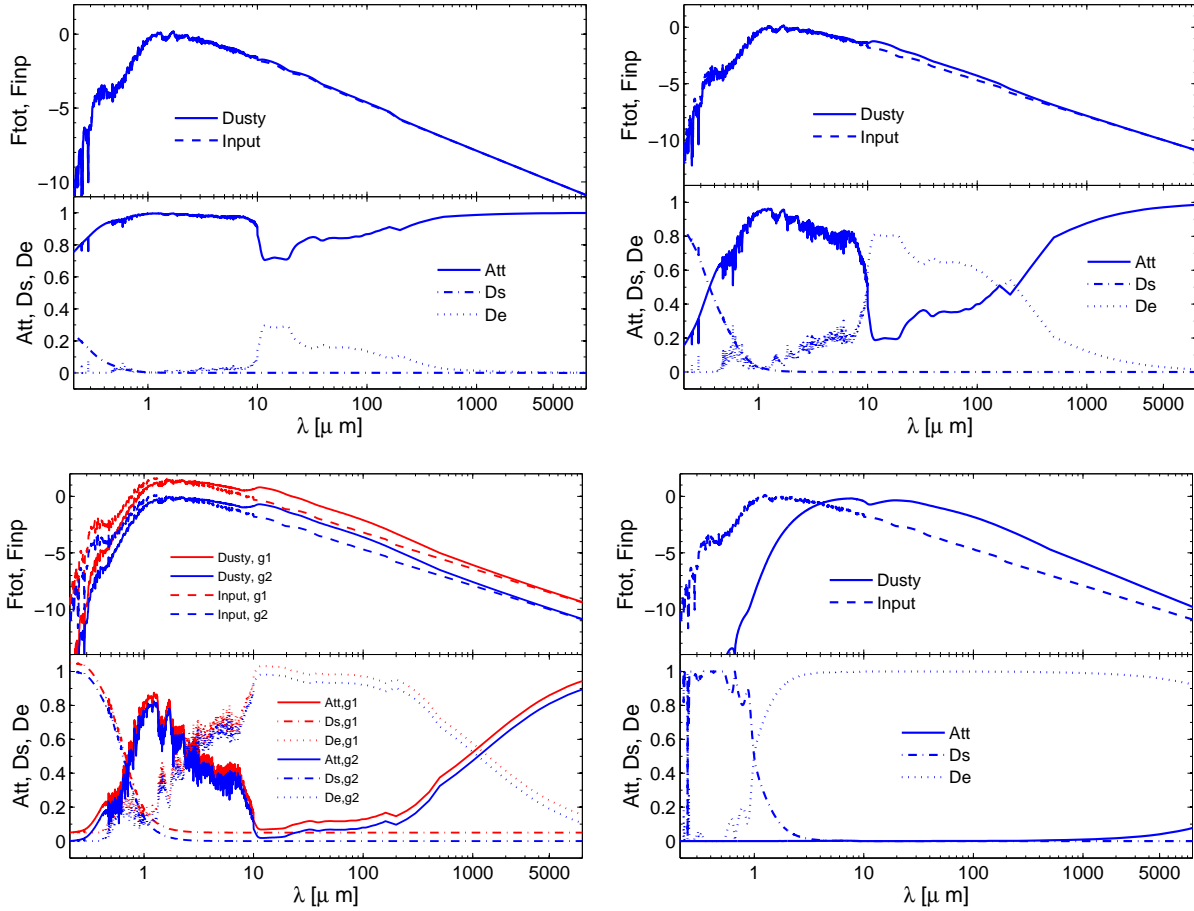


Figure 8. Dust-enshrouded spectra for AGB stars obtained with our modified version of the radiative transfer code DUSTY. The input parameters are: M-type AGB stars with $T_{\text{eff}}=2500$ and $L=3000 L_{\odot}$, oxygen-rich surface composition with 60% Al_2O_3 and 40% silicates. The SEDs for four values of the optical depth are shown: $\tau=0.0224$ (**upper-left panel**), $\tau=0.2083$ (**upper-right panel**), $\tau=1.306$ (**lower-left panel**), and $\tau=30.0$ (**lower-right panel**). The lower-left panel shows the results for two different gravities of the input spectra. More details are given in the text.

the two-fluids medium made of gas and dust, the dust-to-gas ratio can be expressed as (Ferrarotti 2003):

$$\delta = \frac{\dot{M}_d}{\dot{M} - \dot{M}_d} = \frac{\sum_i \dot{M} X_i \frac{A_{d,i}}{n_{d,i} A_i} f_{d,i}}{\dot{M} - \sum_i \dot{M} X_i \frac{A_{d,i}}{n_{d,i} A_i} f_{d,i}} \quad (25)$$

where the summation is over all dust compounds. Simply, $\dot{M} X_i$ is the abundance of the i -th key-element in the wind and $\dot{M} X_i f_{d,i}$ the fraction of the key element condensed into dust. Dividing by $n_{d,i} A_i m_{\text{H}}$, where $n_{d,i}$ is the number of atoms of the key elements required to form one dust unit, and A_i the atomic weight of the i -th element, we get the number of dust units. Finally, multiplying $A_{d,i} m_{\text{H}}$ by the mass of one dust unit, we obtain the total mass of the i -th dust compound. We then divide the AGB evolution into three regions, corresponding to different $[\text{C}/\text{O}]$ -ratios. Following Ferrarotti & Gail (2006), we define two critical carbon abundances: $\epsilon_{C,1} = \epsilon_{\text{O}} - 2\epsilon_{\text{Si}}$ and $\epsilon_{C,2} = \epsilon_{\text{O}} - \epsilon_{\text{Si}} + \epsilon_{\text{S}}$, where $\epsilon = X/A$ is the abundance in mol g^{-1} . The two corresponding critical $[\text{C}/\text{O}]$ -ratios are $([\text{C}/\text{O}])_1 = 0.9$ and

$([\text{C}/\text{O}])_2 = 0.97$. Ferrarotti (2003) groups the stars along the AGB into three classes: M-stars, S-stars and C-stars.

Oxygen-rich M-stars. The spectra of oxygen-rich, M-type AGB stars show two typical features at $10 \mu\text{m}$ and $18 \mu\text{m}$, either in absorption or in emission, depending on the optical depth of the surrounding envelope. These features are usually attributed to stretching and bending modes of Si-O bonds and O-Si-O groups, and probe the existence of silicate grains in the circumstellar shell. Because of the strong bond between O and C in the carbon monoxide, it is believed that all C is blocked into CO molecules and none is available for the formation of dust grain with other chemical species of low abundance. In contrast, the fraction of O not engaged in CO reacts with other elements such as Mg and Si, and forms various types of compounds. Iron dust can accrete onto the envelope as well. By applying Eq. 25 to the specific case we get:

$$\dot{M}_d = \dot{M} \left(X_{\text{Si}} \frac{A_{\text{sil}}}{A_{\text{Si}}} f_{\text{sil}} + X_{\text{Fe}} \frac{A_{\text{iro}}}{A_{\text{Fe}}} f_{\text{iro}} \right) \quad (26)$$

where X_{Si} and X_{Fe} are the mass fractions of the key elements involved (iron for iron dust grains and silicon for silicates),

A_{Si} and A_{Fe} the atomic weights, and A_{sil} and A_{iro} the mass numbers of one typical unit of dust for silicates and iron respectively (Zhukovska, Gail & Tieloff 2008). According to the dust types considered in Ferrarotti & Gail (2006) we have that silicates includes olivines/pyroxenes/quartz: $f_{\text{sil}} = f_{\text{ol}} + f_{\text{pyr}} + f_{\text{qu}}$ and the mean molecular weight of the mixture of silicates is $A_{\text{sil}} = (A_{\text{ol}}f_{\text{ol}} + A_{\text{pyr}}f_{\text{pyr}} + A_{\text{qu}}f_{\text{qu}}) / f_{\text{sil}}$. The total fraction of silicates is calculated following (Ferrarotti 2003):

$$f_{\text{sil}} = 0.8 \frac{\dot{M}}{\dot{M} + 5 \times 10^{-6}} \sqrt{\frac{\epsilon_{\text{C},1} - \epsilon_{\text{C}}}{\epsilon_{\text{C},1}}} \quad (27)$$

where we still need to specify f_{ol} , f_{pyr} and f_{qu} . According to Ferrarotti & Gail (2001), the mixtures depend on the ratio between the abundances of Mg and Si that is about 1.06 for solar abundances (Zhukovska, Gail & Tieloff 2008). For a typical M-star: $f_{\text{ol}}/f_{\text{pyr}}=4$ and $f_{\text{ol}}/f_{\text{qu}}=22$ (Marigo et al. 2008). Finally, for the iron dust:

$$f_{\text{iro}} = 0.5 \frac{\dot{M}}{\dot{M} + 5 \times 10^{-6}} \quad (28)$$

S-stars. S-stars fall into the range $0.90 \leq [\text{C}/\text{O}] \leq 0.97$. With the scarce oxygen available, only iron-dominated dust mixtures are possible. The situation is described by Eqs. (26) and (28). Once more, the silicates are grouped with the same ratios as for M-stars (Ferrarotti & Gail 2002), whereas the condensation fraction is lower than predicted by Eq. (27):

$$f_{\text{sil}} = 0.1 \frac{\dot{M}}{\dot{M} + 5 \times 10^{-6}} \quad (29)$$

Carbon-rich C-stars. According to the scheme adopted, we consider a carbon-rich environment of dust formation when $[\text{C}/\text{O}] \geq 0.97$. When this occurs, the formation of oxygen-rich dust ceases, replaced by carbon-rich compounds, and the C-star phase. Thereinafter, the continuous formation of carbon-rich dust makes the envelopes of these stars increasingly optically thick. By losing mass at very high rates, these stars get enshrouded by thick envelopes that absorb and scatter the UV-optical radiation to the IR and radio wavelengths. According to Ferrarotti & Gail (2006), two types of dust are present: carbonaceous grains, that are the natural product of a carbon-rich environment, and silicon carbide (SiC). Indeed, almost all these stars show an emission feature at $11.3 \mu\text{m}$ due to SiC, whose presence was predicted by Gilman (1969) and observationally confirmed by Hackwell (1972). Applying Eq. (25) to the C-stars we get:

$$\dot{M}_d = \dot{M} \left(X_{\text{C}} \frac{A_{\text{SiC}}}{A_{\text{C}}} f_{\text{SiC}} + X_{\text{C}} f_{\text{car}} \right) \quad (30)$$

with the obvious meaning of the symbols. The terms f_{car} and f_{SiC} are evaluated following Ferrarotti (2003). For f_{SiC} we used Eq. (28), while

$$f_{\text{car}} = 0.5 \frac{\dot{M}}{\dot{M} + 5 \times 10^{-6}} \left(\frac{\epsilon_{\text{C}} - \epsilon_{\text{O}}}{\epsilon_{\text{O}}} \right) \quad (31)$$

Once the dust-to-gas ratio is specified, we have all parameters entering Eq. (14) for the optical depth. We then proceed

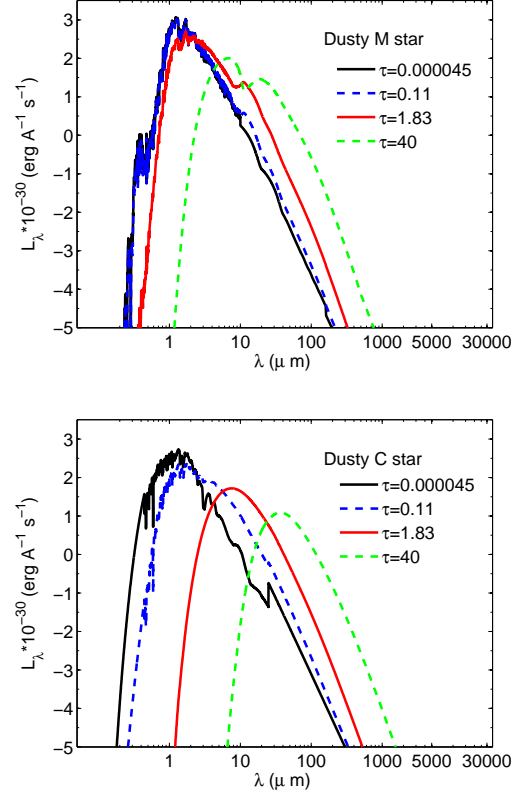


Figure 9. Dust-enshrouded AGB spectra for various optical depths for oxygen-rich M-stars (**top panel**) and carbon-rich C-stars (**bottom panel**).

in the following way: given an AGB star (or an elementary interval of the AGB isochrone) with (L, T_{eff}) and the corresponding surface element abundances, we calculate the SED of the resulting dust-enshrouded object. In brief, for every AGB model or evolutionary track/isochrone elementary interval we need: L , T_{eff} , \dot{M} , the $[\text{C}/\text{O}]$ -ratio and the element abundances at the surface, X_i . This fixes the optical depth τ at the surface and the mixture of dust formed in the envelope, that in turn determine the extinction coefficients Q to be used in the radiative transfer problem. We can thus calculate the final SED to compare with observations.

7 THEORETICAL SPECTRA OF O- AND C-RICH STARS

Our goal is to calculate spectra modified by the effect of the dust shells around the AGB stars. The ideal approach would be to generate for each AGB model the corresponding SED and use it to derive magnitudes and colours in a given photometric system. However, this way of proceeding that was occasionally adopted by Piován, Tantalo & Chiosi (2003) is very time-consuming. It requires solving the radiative transfer problem on a star-by-star basis: it can be applied only if the number of models is small. In the present study, we follow a different approach. We first set up two libraries of dust-enshrouded AGB spectra, one for O-rich and the other for C-rich objects, that cover the full parameter space spanned by our AGB models. Interpolations among

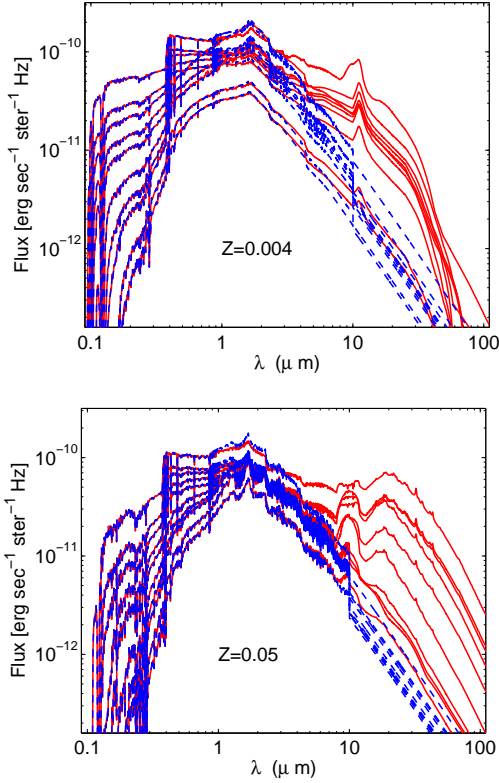


Figure 10. SEDs (F_ν vs. λ) for the SSPs with ages from 0.1 to 2 Gyr. The case with dusty circumstellar envelopes around AGB stars are displayed as red solid lines, while results without dust are plotted with blue dotted lines. Ages range from the oldest (bottom) to the youngest (top) values (2.0, 1.5, 0.95, 0.8, 0.6, 0.4, 0.325, 0.25, 0.15, 0.1 Gyr). The metallicity is $Z=0.004$ (top panel) and $Z=0.05$ (bottom panel).

the library SEDs will provide the spectro-photometric properties of the AGB section of our isochrones. Each library contains 600 spectra. The parameters have been grouped according to:

- **The optical depth.** τ is derived from Eq. (14) using the appropriate physical parameters that describe the central star and the surrounding dust shell. For each group (C-stars and M-stars) we calculate 25 optical depths, going from 0.000045 to 40 (Groenewegen 2006), at a suitable reference wavelength of the MIR, for the chemical mixture that forms the dust.

- **The SED of the central star embedded in the dust-shell.** The total luminosity is not required, a normalized flux $\lambda \cdot F_\lambda$ in some arbitrary units being sufficient. The following SEDs for the central stars are adopted: for the oxygen-rich stars we use the SEDs of the Lejeune, Cuisinier & Buser (1997) library, that includes also semi-empirical spectra of cool M-stars by Fluks et al. (1994); for the C-stars we select a suitable number of SEDs from the Aringer et al. (2009) models of dust-free C-stars. For the M-stars, we adopt six values of the temperature (2500, 2800, 3000, 3200, 3500, and 4000 K), but no specification is made for the gravity, because the sample of Fluks et al. (1994) contains empirical spectra. For the library of C-stars we adopt six values of tempera-

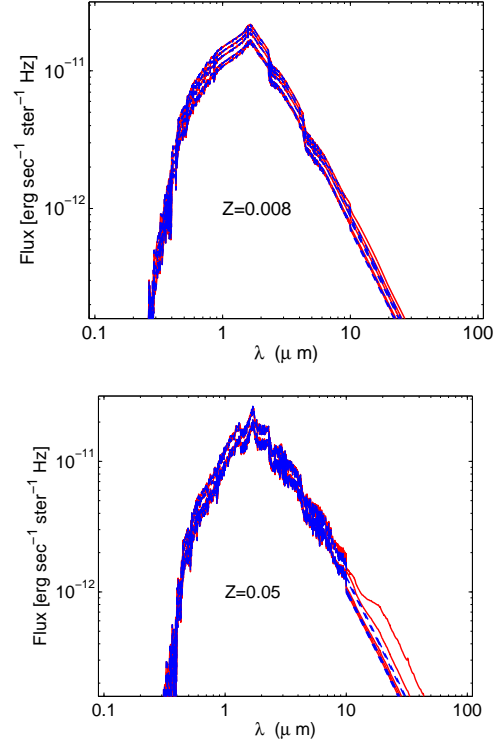


Figure 11. SEDs (F_ν vs. λ) for the SSPs with $Z=0.008$ (top panel) and $Z=0.05$ (bottom panel). Red solid lines correspond to models including dusty circumstellar envelopes, and blue dotted lines to SSPs without dust. From bottom to top the displayed ages are: 6, 7, 8, 9 and 10 Gyr.

ture (2400, 2700, 3000, 3200, 3400, and 3900 K), see also Aringer et al. (2009). We consider two values for the [C/O]-ratio, namely [C/O] = 1.05 and [C/O] = 2. Finally, for the input mass, gravity, and metallicity we use $M = 2 M_\odot$, $\log g = 0.0$, and $Z=Z_\odot$.

- **The composition of the dust in the outer envelope.**

- (i) **C-stars.** Several types of dust grains in carbon-rich AGB stars have been detected by observations: the three main types are amorphous carbon (AMC), silicon carbide (SiC), and magnesium sulphide (MgS). In our models the presence of MgS has been neglected. MgS has been first proposed as a candidate to explain the $30\mu\text{m}$ feature in evolved C-stars by Goebel & Moseley (1985), and this hypothesis has been strengthened by theoretical and observational analyses (see Zhukovska & Gail 2008, for more details). However, according to recent studies, to account for the feature in a typical C-rich evolved object one would require a much higher MgS mass than available (Zhang, Jiang & Li 2009). Also, MgS causes a mismatch between predicted and observed spectral feature (Messenger, Speck & Volk 2013). In addition, the $30\mu\text{m}$ feature is not ubiquitous: it is difficult to determine the ranges of stellar mass and mass-loss where the feature should be included (Zhukovska & Gail 2008), and therefore, in conclusion, we decide to ignore MgS. With respect to AMC and SiC we rely on the results by Suh (2000), who derived new opacities for the AMC that are consistent with the Kramers-Kronig dispersion relations and reproduce the observational data. The models improve upon previ-

ous studies (Blanco et al. 1998; Groenewegen et al. 1998) and are characterized by two components, SiC and AMC. AMC and SiC influence the outgoing spectrum in different ways: whilst the effects of AMC propagate over the whole spectrum, those of SiC are limited to the 11 μm feature, as indicated by the observations. Lorenz-Martins & Lefevre (1994) and Groenewegen (1995) suggest that the ratio SiC to AMC decreases at increasing optical depth of the dusty envelope. According to Suh (1999), for optically thin dust-shells ($\tau_{10} \leq 0.15$, where τ_{10} is the optical depth at 10 μm) the strong 11 μm feature requires about 20% of SiC dust grains to fit the observational data; for dust-shells with intermediate optical thickness ($0.15 \leq \tau_{10} \leq 0.8$) about 10% SiC dust grains are needed, whereas for shells with larger optical depths, where the 11 μm feature is either much weaker or missing at all, no SiC is required. The optical constants of αSiC by Pégourié (1988) are adopted to calculate the opacity of SiC, and according to the above considerations we take two extreme compositions: the first one has 100% AMC only, whereas the second one has 80 % AMC and 20% SiC. The reference optical depth has been chosen at 11.33 μm for the 100% AMC mixture, and at 11.75 μm for the 80 % AMC and 20% SiC mixture (Groenewegen 2006).

(ii) *M-stars*. In the circumstellar environment of M-stars a wide number of dust grains is formed, and a condensation sequence has been proposed by Tielens (1990). At increasing mass-loss the dust composition changes from aluminium and magnesium oxides rich at low \dot{M} , to a mixture with both oxides and olivines, and finally to a composition dominated by the silicates, with amorphous silicates and crystalline silicates at high \dot{M} . This sequence seems to be able to reproduce the changes observed in the shape of the 10 μm feature. Even if this scheme is still a matter of debate (van Loon et al. 2006), it is consistent with the observations of different types of stars at different metallicities (Dijkstra et al. 2005; Heras & Hony 2005; Lebzelter et al. 2006; Blommaert et al. 2006). We adopt the above sequence as a plausible scenario for the condensation of dust in oxygen-rich stars. Three possible compositions are included: (1) pure Al_2O_3 with optical properties taken from Begemann et al. (1997); (2) mixed composition with 60% Al_2O_3 and 40% silicates, with the optical properties taken from David & Pegourie (1995); (3) 100% silicates for high mass-loss rates, with two possible choices, i.e. either a complete composition with optical properties from David & Pegourie (1995) for comparison with Groenewegen (2006), or a more elaborate description based upon Suh (1999, 2002). The latter author adopted different silicates opacities at varying 10 μm feature, namely cold and warm silicates. The model then has been refined by Suh (2002) taking into account crystalline silicates through the so-called crystallinity parameter α , because in many AGB stars with high mass-loss rates, ISO hi-resolution observations reveal the presence of prominent bands of crystalline silicates, like enstatite (MgSiO_3) and forsterite (Mg_2SiO_4) (Waters et al. 1996; Waters & Molster 1999). The adopted opacity functions for these latter are taken from Jaeger et al. (1998). Following Piovan, Tantaló & Chiosi (2003), we adopt here $\alpha = 0.1$ for stars with low mass-loss rates and moderately optically thick shells ($\tau_{10} < 15$), whereas for oxygen-rich stars with high mass-loss rates and very thick shells ($\tau_{10} > 15$) we prefer the value $\alpha = 0.2$. Finally, in all models

the relative contents of enstatite (MgSiO_3) and forsterite (Mg_2SiO_4) are the same as in Suh (2002). Finally, we take also into account the recent results by McDonald et al. (2011). They found that metallic iron seems to dominate the dust production in metal-poor oxygen-rich stars. We therefore adopt a 100% iron mixture to simulate the envelope of metal-poor stars surrounded by a thin dust shell. The optical properties of iron are taken from Ordal et al. (1988). The following reference wavelengths are adopted for the grid of τ : 11.75 μm for both pure aluminum oxides and oxides plus silicates, and 10.20 μm for both pure silicates cases. All the above opacities are used as input for DUSTY. This radiative transfer code then applies the Mie theory to calculate scattering and absorption efficiencies by a homogeneous spherical sphere. The grain size distribution is chosen between the options available in DUSTY (Ivezic & Elitzur 1997). In particular, we adopt single size grains with dimension $a=0.1\mu\text{m}$ (see Piovan, Tantaló & Chiosi 2003, for more details about this choice). An analytical dust density profile, suitable for the modelling of AGB stars, is also selected from the available options. This profile is appropriate in most cases and offers the advantage of a much reduced computational time (see DUSTY manual at the url <http://www.pa.uky.edu/~moshe/dusty/>). The envelope expansion is driven by radiation pressure on the dust grains.

- **The temperature T at the inner boundary of the dust shell.** For this parameter we assume either 1000 K or 1500 K, depending on the type of dust (Piovan, Tantaló & Chiosi 2003).

- Finally, we comment on the luminosity of the central star. For C-stars we keep the luminosity specified by Aringer et al. (2009). Given that Fluks et al. (1994) does not specify the luminosity of the M-stars producing the empirical spectra, but gives only the specific intensity, we fix the luminosity of the M-stars at $L=3000L_\odot$. The library of dusty stellar spectra is therefore calculated for a fixed luminosity of the underlying objects. This is not a problem, for the luminosity does not affect the solution of the radiative transfer (Ivezic & Elitzur 1997) and the shape of the outgoing SEDs. The resulting flux is scaled to the real luminosity of the AGB star we are considering.

Figure 8 displays the SEDs of O-rich AGB stars of our template library, for four values of the optical depth. The input parameters are: $T_{\text{eff}}=2500$ and $L=3000L_\odot$ of the central star, optical depths $\tau=0.0224$, 0.2081, 1.306 and 30.0, and dust composition according to the second prescription for oxygen-rich stars (60% Al_2O_3 and 40% silicates). The lower-left panel shows the results for two different gravities ($\log g=-1.02$ and $\log g=0.5$) of the input spectrum from the Fluks et al. (1994) compilation. For the sake of clarity, the two SEDs are artificially shifted by a small amount, otherwise the two spectra would be coincident. Indeed, as expected and tested, there is no dependence on the gravity in the Fluks et al. (1994) spectra. The stellar features in the UV-optical-near IR region disappear with increasing optical depth, and an increasingly featureless SED appears: this is ultimately due to the smooth optical properties of the selected composition. The stellar light is shifted more and more toward longer wavelengths; for the lowest optical depths the input and output spectra are almost coincident, while the effect of dust is apparent for the largest values of

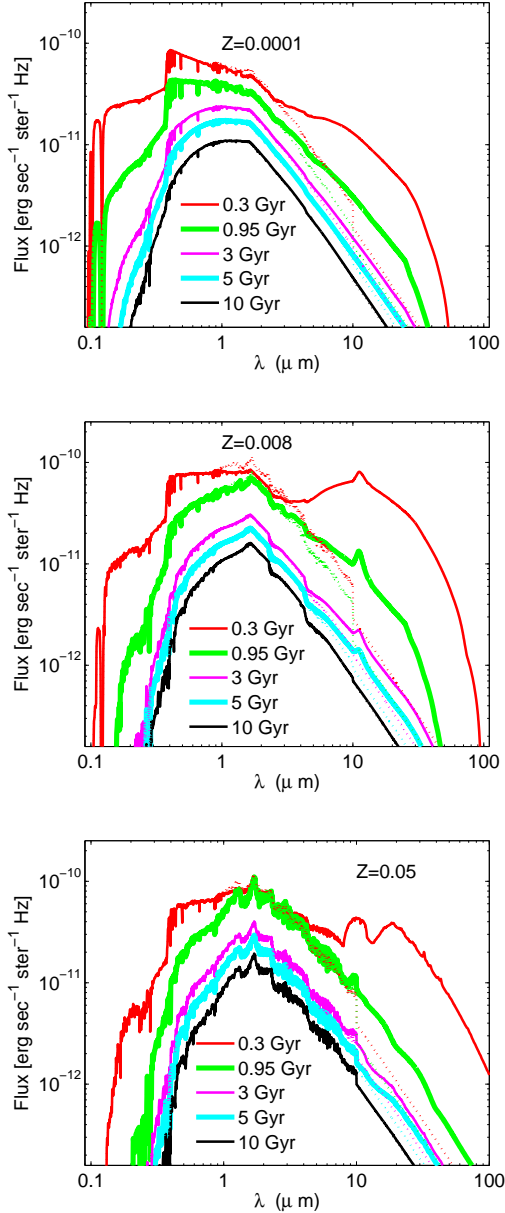


Figure 12. Detailed comparison of SEDs for old SSPs (dotted lines) and new SSPs (solid lines), for the labelled ages and metallicities. Three metallicities are shown: $Z=0.0001$ (top panel), $Z=0.008$ (middle panel) and $Z=0.05$ (bottom panel).

τ . In the lower panels we show: the fractional contribution of the attenuated input radiation to the total flux (labelled as Att – solid lines); the fractional contribution of the scattered radiation to the total flux (labelled as Ds – dot-dashed lines), and finally the fractional contribution of the dust emission to the total flux (labelled as De – dotted lines). As expected, at increasing optical depth τ (i) the fraction of not attenuated or scattered light escaping the dust-shell decreases, and (ii) the dust contribution becomes significant at $\tau \sim 0.2$ and dominant at $\tau \sim 1$.

Finally, Fig. 9 shows a sequence of obscured spectra of AGB stars at increasing optical depth, both for O-rich (top

panel) and C-rich (bottom panel) stars. It is evident how the SEDs progressively shift towards longer wavelengths with increasing τ . The spectra with 100% AMC dust composition represent a limiting case with no SiC feature at $11.3 \mu\text{m}$. It is worth noticing that for the oxygen-rich stars, when the optical depth is very high, the silicate feature at $9.7 \mu\text{m}$ appears in absorption as indicated by the observational data (Suh 1999, 2002).

8 SEDS AND COLOURS OF SSPS WITH DUST ENSHROUDED AGB STARS

With our new isochrones and library of dust-enshrouded AGB stars we have calculate the SEDs of SSPs. Figure 10 displays the SEDs with (red lines) and without (blue lines) dust-enshrouded AGB stars for different ages and metallicities $Z=0.004$ and $Z=0.05$, respectively. Ages range from 0.1 to 2 Gyr and correspond to young and intermediate-age SSPs. The effect of the dust-enshrouded AGB stars is remarkable and cannot be neglected in the region from NIR to FIR. Figure 11 shows the SEDs for old ages from 6 to 10 Gyr, metallicities $Z=0.008$ and $Z=0.05$, respectively. For old ages the effect of dust-enshrouded AGB stars is small, mainly because of the short duration of the AGB phase (only a few thermal pulses) due to of the low total mass along the AGB. Only for the highest metallicity $Z=0.05$ the dust surrounding AGB stars has some effect on the SED. Another example of the effect of the dust-shells around AGB stars is shown by Fig. 12, that compares the new and old SEDs for a few selected ages and for three metallicities, e.g. $Z=0.0001$, $Z=0.008$ and $Z=0.05$. Similar results are found for all the remaining metallicities.

The old spectra without dust shells do not extend into the NIR and FIR, but decline sharply at wavelengths longer than about $3\text{--}4 \mu\text{m}$. The spectra of the new SSPs, instead, extend towards long wavelengths, and the amount of flux in the MIR and FIR is significant. Differences start at about $1 \mu\text{m}$; in the IR range up to $3\text{--}4 \mu\text{m}$ the flux of dusty SSPs is lower than the old one, due to the fact that dusty envelopes shift the emission of M- and C-stars towards longer wavelengths. It is worth noticing the evolution of the features of silicon carbide at $11.3 \mu\text{m}$, and amorphous silicate at $9.7 \mu\text{m}$, at different metallicities. The amount of energy shifted to longer wavelengths is larger for the young ages, because of more massive and luminous AGB. Considering the different metallicities, we note the following effects:

- $Z=0.0004$ and $Z=0.0001$: for stars of very low metallicity the TDU is particularly efficient during the AGB phase in enriching the surface with ^{12}C and other products of He-burning. These stars display a C-rich surface for most of their evolution. The presence of dusty C-rich stars in young SSPs leads to featureless SEDs dominated by amorphous carbon. The small amounts of metals in the envelope inhibit high optical depths, and the amount of radiation re-emitted in the MIR/FIR region is smaller than in case of higher metallicities.

- $Z=0.004$ and $Z=0.008$: for most of the age range covered by the models, the spectrum does not show the features due to amorphous and crystalline silicates, because C-stars dominate (the $11.3 \mu\text{m}$ feature of SiC is indeed prominent). This is quite different from the results

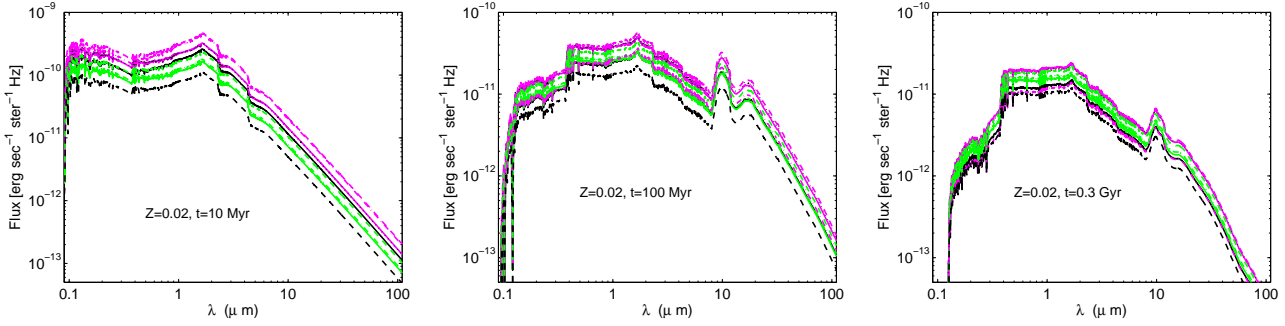


Figure 16. Comparison between the new dusty SEDs, at varying age and IMF. The metallicity is $Z=0.02$. Three ages are considered: $t=10$ Myr (**left panels**), $t=100$ Myr (**middle panels**), and $t=300$ Myr (**right panels**). Each line corresponds to a different IMF, according to the line-style and colour code of Fig. 3. Very similar curves are found for all other metallicities.

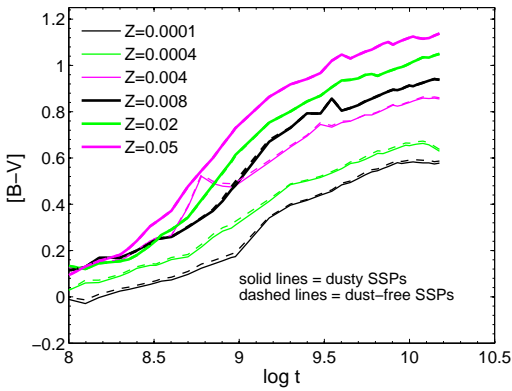


Figure 13. Integrated $[B-V]$ colour of SSPs as a function of age, in the range from 0.1 to 15 Gyr, for the whole metallicity grid. Solid lines denote the SSPs with *dust-free* AGB stars, dashed lines colours including *dust enshrouded* AGB stars. The unit of time t is yr.

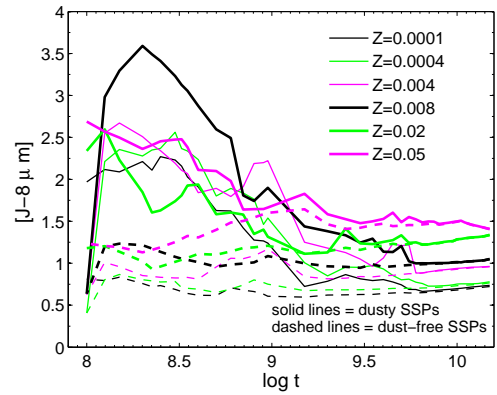


Figure 15. As in Fig. 13, but for $[J - 8 \mu m]$

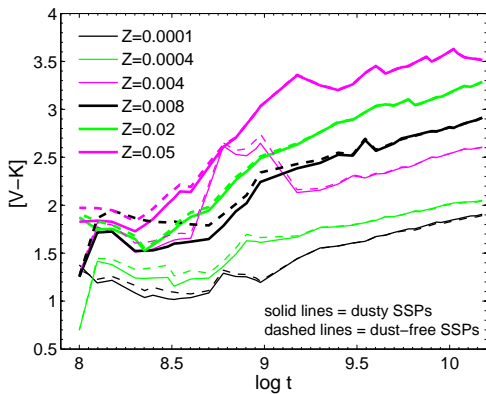


Figure 14. As in Fig. 13, but for the integrated $[V-K]$ colour.

by Piován, Tantalo & Chiosi (2003), where the oxygen-rich phase at these metallicities played an important role, and a significant evolution of the MIR features was present. In Piován, Tantalo & Chiosi (2003), C-stars dominated for young ages, whereas for intermediate ages (around 3 Gyr),

the O-stars of low optical depth contributed to the integrated spectrum and the $9.7 \mu m$ feature could be seen in emission. Finally, for even older ages the high optical depth O-stars dominated, such that the spectrum became more articulated and the features due to crystalline silicates started to appear in the IR. All this does no longer occur (for metallicities in this range), simply because the evolution of the $[C/O]$ -ratio in the Weiss & Ferguson (2009) models of AGB stars leads to a different path. Furthermore, it must be noted that, compared to Piován, Tantalo & Chiosi (2003), the amount of flux shifted towards longer wavelengths is generally smaller. This is due to the lower optical depths, now more realistically linked to the composition and mass-loss of the underlying star. Finally, the present optical depths agree well with those of Groenewegen (2006) for similar mass-loss rates.

- $Z=0.02$: for the youngest ages, C-stars appear in a narrow luminosity range (Fig. 5), and the stars at the AGB tip, with the highest mass-loss rate and the highest optical depth, are O-stars. The SSP spectrum is dominated by the $9.7 \mu m$ feature, that appears in emission and not in absorption, as expected in envelopes with rather small optical depths. No features of crystalline silicates show up in the spectrum, because according to the models by Suh (2002) much higher optical depths would be required.

- $Z=0.05$: AGB stars of super-solar metallicities dis-

play only oxygen-rich surfaces (Fig. 5) and do not reach the carbon-rich phase in the models by Weiss & Ferguson (2009). At 0.3 Gyr and for young ages (see Fig. 12), the SSPs spectra display both amorphous silicates (at $\sim 10 \mu\text{m}$) and features due to crystalline silicates ($\sim 30 \mu\text{m}$) because of the high optical depths.

8.1 SSP colours

SEDs and colours of SSPs have a strong dependence on age, metallicity and the presence of dust shells around the AGB stars. This is clearly demonstrated by Figs. 13, 14 and 15 for the $[B - V]$, $[V - K]$ and $[J - 8\mu\text{m}]$ colours. The age range considered covers the onset of the AGB phase until the very old ages when the contribution of AGB stars to the integrated flux is very low. As well known, age and metallicity – this latter enhanced by the effects of AGB dust-shells – drive the evolution of the SSP colours.

The peak emission of the central AGB stars surrounded by dust shells is at around $1\text{--}2 \mu\text{m}$; the dust shifts the flux from J , H and K bands to longer wavelengths. This effect is stronger at shorter wavelengths (J -band) than at the longer ones (like K -band). It is the combination of this effect together with the exact position of the emission peaks of the central stars that determine the increase of the IR magnitudes. Depending on the age and metallicity of the population, the net effect is that sometimes the J magnitude increases more than the K magnitude, while in other cases the opposite effect is true. It is in the Spitzer $8 \mu\text{m}$ pass-band that we mostly see the radiation emitted by dust around AGB stars. Even the coolest AGB star would provide a negligible contribution to that band if the dust shells are ignored. For the $[V - K]$ colour, dust mainly makes the K magnitude fainter, and affects only slightly the V flux, producing overall bluer colours. The effect of dust is small in the UV/optical pass-bands (see Fig. 13), and the $[B - V]$ colours are practically unaffected by the presence of the dust surrounding AGB stars.

8.2 SEDs and colours of SSPs for variations in the IMF

Recalling the definition of the monochromatic flux emitted by an SSP of age t and metallicity Z , the choice of an IMF implies that along the corresponding isochrone, between M_l and $M_u(t)$ (the most massive living stars at that age), the relative number of stars per mass intervals dM is defined. The mass range spanned by all evolutionary stages beyond the main sequence turn-off decreases from a few solar masses to a few hundredths of a solar mass as the age increases from very young (a few Myr) to very old (a few Gyr). This means that but for very young SSPs, changing the IMF has little impact on the integrated magnitudes and colours of SSPs. Main sequence stars that are one or two magnitudes fainter than the turn-off contribute significantly to the SSP mass, but little to magnitudes and colours.

In relation to this, we recall that the various IMFs do not have the same M_l and do not predict the same percentages of stars and hence stellar mass in different mass intervals. Looking at the entries of Table 1, $\text{IMF}_{\text{Kro-27}}$, $\text{IMF}_{\text{Lar-MW}}$, $\text{IMF}_{\text{Lar-SN}}$, IMF_{Cha} , and IMF_{Ari} are all defined down to a lower mass limit of $0.01 M_\odot$, whereas

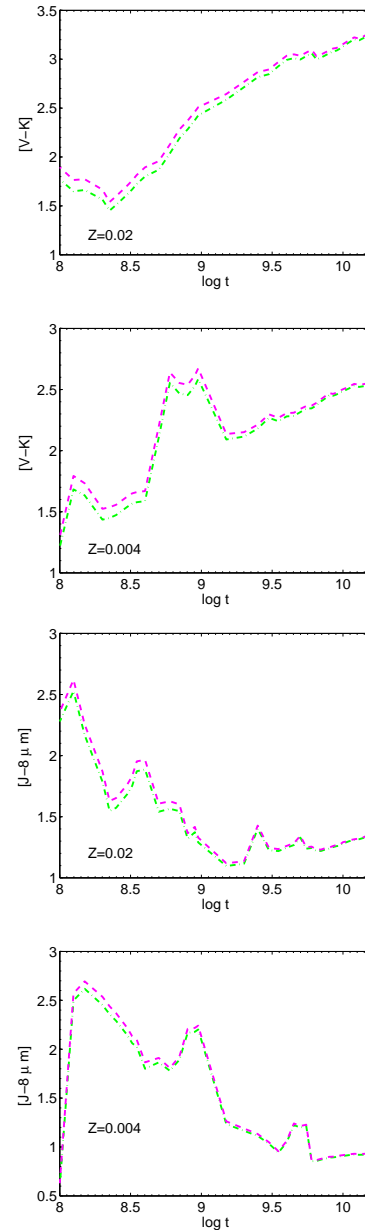


Figure 17. Theoretical $[V - K]$ and $[J - 8 \mu\text{m}]$ colours as a function of age (from 0.1 to 15 Gyr) for the labelled metallicities, and the two IMFs that cause the most extreme variations: results for the other IMFs discussed in this paper lie between the lines displayed. Colour and line-style for the results with different IMF are as in the Fig. 3. Time t is again in yr.

the remaining ones have a lower mass limit of $0.1 M_\odot$ (Piovan et al. 2011). Some IMFs, like $\text{IMF}_{\text{Kro-Ori}}$, and IMF_{Sca} , predict a number fraction of massive stars – including SNe – much smaller than the number fraction of AGB stars. Others, like $\text{IMF}_{\text{Lar-MW}}$, IMF_{Kenn} , and IMF_{Cha} behave in a different way and, even if again they predict a fractional mass of AGB stars higher than that of SNe, the relative contribution of SNe is much more significant. Only for the peculiar IMF_{Ari} the trend is reversed and SNe outnumber AGB stars. The different number ratios of stars going through the AGB to stars that become SNe have two

Table 2. Ratios of the integrated fluxes predicted by several IMFs to the Salpeter IMF. Two metallicities are considered: $Z=0.004$ and $Z=0.02$. Three ages are displayed: $t=10$ Myr, $t=100$ Myr, and $t=300$ Myr. All SSP fluxes are normalized to a total SSP mass of $1 M_{\odot}$. Given that for a given IMF, Z and age the ratios depend on the wavelength, we display for each case the minimum and maximum values.

Age (Myr)		10	10	100	100	300	300
Metallicity Z		0.004	0.02	0.004	0.02	0.004	0.02
Larson Solar Neighbourhood	IMF _{Lar-SN}	0.87–0.99	0.90–1.05	1.33–1.41	1.29–1.42	1.46–1.55	1.44–1.54
Larson (Milky Way Disc)	IMF _{Lar-MW}	1.79–1.81	1.77–1.81	1.69–1.71	1.67–1.72	1.59–1.66	1.60–1.68
Kennicutt	IMF _{Kenn}	1.22–1.30	1.24–1.34	1.50–1.57	1.49–1.58	1.58–1.67	1.58–1.67
Kroupa (original)	IMF _{Kro-Ori}	0.61–0.70	0.63–0.76	1.00–1.09	0.97–1.04	1.13–1.27	1.10–1.26
Chabrier	IMF _{Cha}	1.18–1.33	1.22–1.38	1.57–1.61	1.58–1.61	1.58–1.62	1.59–1.63
Arimoto	IMF _{Ari}	1.80–1.57	1.48–1.74	1.10–1.01	1.00–1.14	0.86–0.96	0.87–0.98
Kroupa 2002-2007	IMF _{Kro-27}	0.66–0.76	0.68–0.82	1.08–1.18	1.05–1.19	1.22–1.37	1.19–1.35
Scalo	IMF _{Sca}	0.42–0.48	0.43–0.51	0.69–0.74	0.66–0.75	0.77–0.86	0.75–0.85

effects. First, we expect that for the IMFs with a greater AGB mass fraction the effect of AGB circumstellar dust on magnitudes and colours is more significant than in the other cases. Second, the IMF choice affects the amount of dust injected into the ISM. Before the main process of dust formation happens in the ISM, the partition between AGB and SNe drives the amounts of star-dust injected into the ISM (Zhukovska, Gail & Tieloff 2008; Piován et al. 2011). In each generation of stars, the dust production by either SNe or TP-AGB stars therefore depend on the IMF.

Small differences in the IMFs shown in Fig. 3, especially for $M > 10 M_{\odot}$, have a significant effect on young SSPs. To illustrate this point we calculate the SEDs of SSPs with different chemical composition and age, for all the IMFs listed in Table 1 and for the metallicities $Z=0.004$ and $Z=0.02$. The SEDs are presented in Fig. 16 for three selected ages, namely 10, 100, and 300 Myr, and are limited to a metallicity of $Z=0.02$ (similar results are found for the other metallicities). First of all, the SEDs run nearly parallel for the full wavelength range of interest. We therefore expect the ratio of the flux $F_{\lambda}(\lambda, IMF_1)/F_{\lambda}(\lambda, IMF_2)$ between the SEDs of any two IMFs to remain similar over most of the spectrum. This is shown by the entries of Table 2 that lists the fluxes predicted by our IMFs for the three selected ages presented in Fig. 16, two metallicities and a total mass $M_{SSP}=1 M_{\odot}$, normalized to the values predicted by the Salpeter IMF. For each case, the minimum and maximum flux ratios obtained across the wavelength range from 0.1 to 100 μm , are displayed.

Looking at the entries of Table 2, we see that IMF_{Ari} and IMF_{Lar-MW} predict the largest SSP fluxes for the youngest age, followed by IMF_{Kenn} (IMF_{Cha} is practically coincident with IMF_{Kenn}), in agreement to what is suggested by Fig. 3. IMF_{Ari} and IMF_{Lar-MW} indeed present the greatest fractional mass contribution of high-mass stars. At SSPs ages $t=100$ Myr and 300 Myr, IMF_{Kenn}, IMF_{Lar-MW} and IMF_{Cha} have the highest flux ratio (as expected from the entries of Table 1). These IMFs predict the greatest fraction of stars with mass between $1 \leq M_{\odot} < 6$. The same trend is visible for $Z=0.004$. For the ages considered, IMF_{Sca} predicts the lowest SSP flux. It has a very small fraction of massive stars, favouring low-mass stars in comparison to the other IMFs: in fact, 68% of the mass is contained in stars with $M < 1 M_{\odot}$ (see Table 1). This causes, as discussed, a lower integrated flux (see the panels of Figs. 16).

We now turn to colours like $[V - K]$ and $[J - 8 \mu\text{m}]$

that are affected by AGB stars. Figure 17 shows that the effect of the IMF is stronger for the youngest ages where an AGB is present, up to 0.2 mag in $[V - K]$. For the oldest ages, changing the IMF does not affect significantly the integrated colours of the SSPs. For both metallicities ($Z=0.02$ and $Z=0.004$ – the remaining ones behave in the same way), when AGB stars appear at approximately $\log t=8$, the IMF_{Lar-MW} predicts the reddest $[V - K]$ colour, whereas the IMF_{Kro-27} predict the bluest one. This is due to the combined effect on the K band of the varying fractional mass of AGB stars and the circumstellar dust. The former effect dominates and makes the colour redder; it is increasing when going from IMF_{Kro-27} to IMF_{Lar-MW}. The effect of circumstellar dust effect is less important and opposite. As we have seen, while the V magnitude is not affected by circumstellar dust, the K magnitude is influenced, producing bluer colours (see Fig. 14). In case of the $[J - 8 \mu\text{m}]$ colour, different IMFs do not change appreciably its evolution and the effect is even smaller than in $[V - K]$.

Finally, the effect of the IMF on the SED of SSPs does not depend appreciably on the chosen metallicity. This is shown by the entries in Table 2: the ratios are almost identical for both metallicities at all ages considered.

9 COMPARING THEORETICAL RESULTS WITH OBSERVATIONS

The key quantities to determine from the analysis of a stellar system are age and metallicity distribution of the parent stars, to reconstruct the star formation and chemical enrichment history of the whole population. A widely used method to determine age and metallicity of unresolved stellar systems is to compare their observed colours with the predictions of EPS models (see Bressan, Chiosi & Fagotto (1994), Tantalo et al. (1998), Bruzual & Charlot (2003), Buzzoni (2005), Piován, Tantalo & Chiosi (2006a,b), Galliano, Dwek & Charnial (2008), and Popescu et al. (2011) just to mention a few). If instead the stellar populations can be resolved into single stars, the star-by-star EPS technique enables one to build synthetic CMDs (Chiosi, Bertelli & Bressan 1986; Bertelli et al. 1994; Aparicio & Gallart 2004; Chung et al. 2013) to derive the star formation history of the population under scrutiny.

To this aim, we wish to validate the new SSPs and study the effect of the new AGB models and the libraries of

dusty AGB spectra, by means of comparisons with observed magnitudes and colours of resolved and unresolved stellar populations. The ideal laboratory for this are both the massive star clusters and the rich CMDs of field stars of the Magellanic Clouds, that host significant populations of intermediate-age, populations not easily accessible in the Milky Way (Pessev et al. 2008).

Due to the large number of studies on the subject, no attempt is made here to summarize previous work, and we will limit ourselves to mention only the sources of the data used in our analysis. Particularly interesting are data in the NIR region of the spectrum, because they allow to, at least partially, break the age-metallicity degeneracy of the integrated colours, especially for stellar populations older than ~ 300 - 400 Myr (Goudfrooij et al. 2001; Puzia et al. 2002; Hempel & Kissler-Patig 2004; Pessev et al. 2006, 2008). In the following, we compare our theoretical models with:

- CMDs of field stars in the Large and Small Magellanic Clouds (LMC and SMC respectively);
- broad-band colours of star clusters in the LMC and SMC, using SEDs with and without *AGB dust shells*.

9.1 Field Stars of the Magellanic Clouds

We compare here selected CMDs of Magellanic Clouds' fields, with our isochrones with and without AGB dust shells. The best available data come from extensive near and mid-infrared surveys like SAGE (*Surveying the Agents of Galaxy Evolution*) (Blum et al. 2006; Bolatto et al. 2007), that matches IRAC (or MIPS) data with 2MASS photometry. The survey has been described by Meixner et al. (2006).

CMDs of Field Stars. We start comparing the CMDs in NIR and MIR photometry, with both our new and old isochrones, for ages in the interval between $t=0.09$ Gyr and 2 Gyr. We consider a metallicity $Z=0.008$ for the LMC, and $Z=0.004$ for the SMC.

Large Magellanic Cloud. For the LMC we adopt a standard distance modulus of 18.5 mag (Pessev et al. 2008). Following Marigo et al. (2008), the data have been limited to a circular area of π square degrees, centred on the LMC bar ($\alpha_{2000} = 5^h 23^m.5$, $\delta = -69^\circ 45'$), to include thousands of bright AGB stars and exclude foreground stars likely belonging to the Galactic Disk (Marigo et al. 2008). The observed CMDs are shown in the various panels of Figs. 18 and 19. A nearly vertical blue plume is always present, probably due to foreground stars of the Galaxy. There is also some contamination in the bottom right part of the CMDs, likely caused by background galaxies. Moreover, in Fig. 19, the objects with roughly $[3.6 - 8] \gtrsim 2$ (the vertical finger in the bottom right part of the CMD) are not detected by 2MASS; they are probably background galaxies and young pre-main sequence stars. The top panels refer to the new isochrones, whereas the bottom panels are for the old ones. The isochrone ages are given at the top of each panel. The most remarkable feature is the much wider extension of the new AGB phase, in better agreement with the observations.

Small Magellanic Cloud. For the SMC we adopted a distance modulus of 19.05 mag (Pessev et al. 2008), and the CMDs are shown in Figs. 20 and 21. The contamination by objects not belonging to the SMC is visible also in this case, due to the same type of stars as for the LMC. Finally, like

in the LMC, objects with roughly $[3.6 - 8] \gtrsim 2$ in Fig. 21, are not detected by 2MASS.

Discussion of field star CMDs. All CMDs of the LMC and SMC field stars, show the clear effect of the dusty circumstellar shells around AGB stars on NIR and MIR colours. Without dust, the theoretical colours are *not able* to reproduce the observed AGB populations. In fact, without dust the AGB phase does not extend towards very red colours, as observed.

In general, isochrones of the appropriate age reproduce the observed AGB sequences, even though in some cases we do not have an exact match. The reason is the too coarse grid of ages we are using. Nevertheless, the fit of the observed CMDs with synthetic CMDs generated with population synthesis techniques is beyond the aims of this study. For our purposes, it is enough to test whether the new isochrones (and SSPs) can cover the observed colour range of AGB stars. By inspecting the various CMDs we draw the following conclusions:

- at very young ages ($\log t=7.95$; the yellow line on the upper-left corner of the CMDs, well visible in all CMDs except in Figs. 19 and 21), AGB stars are not present. The most prominent NIR emitters are the red supergiant stars.
- in the age range $8.10 \leq \log t \leq 8.90$ the TP-AGB phase is well developed. This is the age range in which AGB models best reproduce the red tail of carbon-rich stars. For these metallicities the intermediate-mass stars develop an extended carbon-rich envelope during the AGB phase. The duration of the carbon-rich phase is determined by the interplay between dredge-up and mass-loss. As already pointed out, the efficiency of the TDU increases with decreasing metallicity; it is very efficient for the compositions we are considering.
- for ages in the range $9.18 \leq \log t \leq 9.30$ the TP-AGB phase gets shorter: the carbon-rich envelope is less important, even if its contribution to the red tail is still relevant.

The agreement between our new models and observations is satisfactory for most of the CMDs, and is a significant step forward towards a more realistic description of AGB stars. Similar results have been obtained by Marigo et al. (2008) using synthetic TP-AGB models and a library of dusty spectra of AGB stars. We may also observe that our isochrones, thanks to the new libraries of spectra for M- and C-stars, have a more regular behaviour in the CMDs compared to those of Marigo et al. (2008). This is likely due to the different optical depths adopted for the models (in particular different recipes for the mass-loss rate).

Only in the 2MASS $[K_s]$ vs. $[J - K_s]$ CMDs the models did not match the data satisfactorily. Our AGB isochrones bend towards fainter K_s magnitudes and redder $[J - K_s]$ colours more than the observations, that would suggest a nearly constant K_s . It is hard to trace back the reasons for the discrepancy, considering that in all other NIR/MIR bands the agreement is very good. It could be due to some unrealistic absorption effect in the K_s -band. Work is in progress to clarify this issue.

9.2 Integrated Colours of Star Clusters and SSPs

We compare now our models with integrated photometry of star clusters. Figures 22 and 23 show the time evolution of

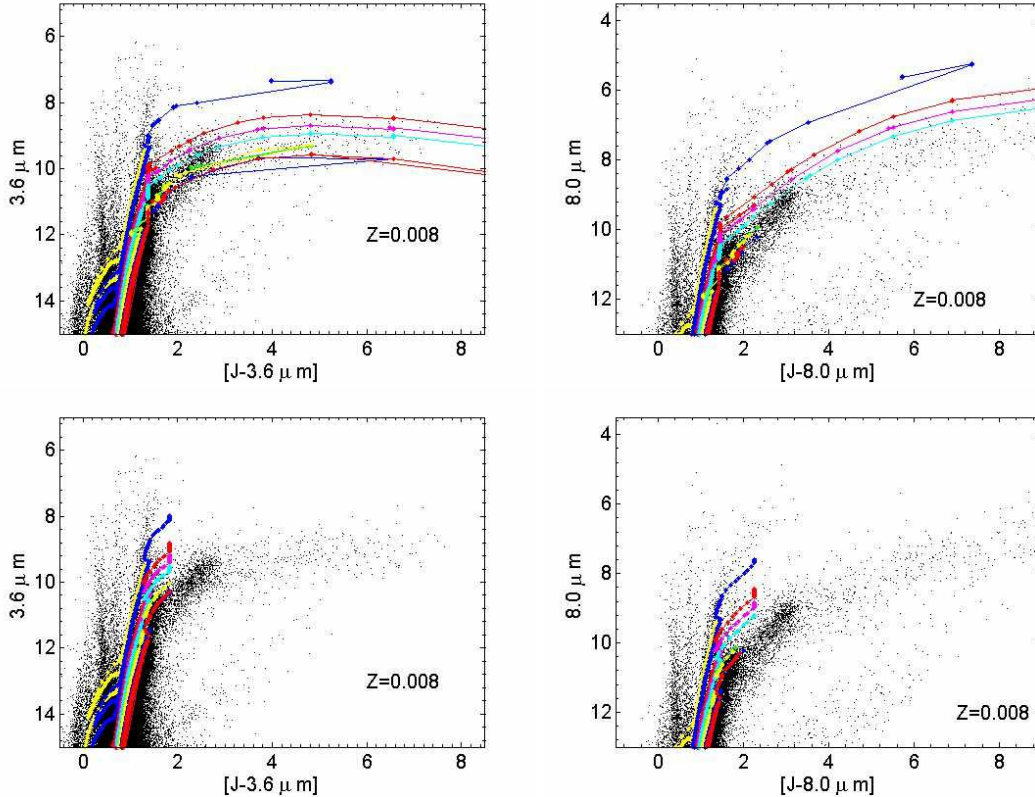


Figure 18. Field stars of the LMC in the 2MASS+IRAC surveys: The $[3.6 \mu\text{m}]$ vs $[J - 3.6 \mu\text{m}]$ (**left panels**) and $[8 \mu\text{m}]$ vs. $[J - 8 \mu\text{m}]$ (**right panels**) CMDs are compared to isochrones with metallicity $Z = 0.008$, representative of the LMC composition. The isochrones are displayed in different colours according to their age ($\log t = 7.95, 8.10, 8.48, 8.60, 8.70, 8.90, 8.95, 9.18, 9.30$, with t in yr. The oldest isochrones are in the bottom right part of each CMD). The top panels show isochrones including AGB dust shells. The bottom panels show models without circumstellar dust shell.

theoretical $[V - K_s]$ and $[J - K_s]$ colours for SSPs with and without the contribution of dusty shells. They are superimposed on optical and near-infrared colours of LMC star clusters, taken from the database by Pessev et al. (2006, 2008).

Recently Pessev et al. (2006, and references therein) presented integrated NIR magnitudes (J , H , K_s) and colours for a large sample of star clusters in the LMC and SMC, using 2MASS data. These clusters have a good estimate of both age and metallicity, and can be used as a calibration set for SSPs models. Many clusters have ages in the age range between 0.3 and 3 Gyr, and consequently their integrated properties are heavily affected by AGB stars, that are extremely luminous in the NIR (Pessev et al. 2006). Pessev et al. (2008) combined these data with new photometry for nine additional objects: the whole resulting set forms the largest existing database of integrated NIR magnitudes and colours of LMC/SMC star clusters. Moreover, the 2MASS data have also been merged with optical photometry from the works by Bica et al. (1996) and van den Bergh (1981). This data set provides a very good coverage of the age-metallicity parameter space of LMC/SMC star clusters.

As in similar studies by Elson & Fall (1985b,a, 1988), Chiosi, Bertelli & Bressan (1986, 1988), Girardi et al. (1995), and Pessev et al. (2008), we compare theoretical predictions and observed cluster colours as a function of age, to test the models, to single out possible ages where dis-

crepancies do appear, and to study the evolutionary history of the photometric properties of a star cluster. As pointed out long ago by Chiosi, Bertelli & Bressan (1986, 1988) and more recently by Pessev et al. (2008), the comparison between theory and observations yields good results only when stochastic effects on the integrated colours are taken into account. The issue is the following: the calculation of integrated properties of SSPs assumes that all stellar evolutionary phases are well sampled. Therefore, a model will match the observations only if the observed integrated magnitudes/colours sample a number of stars large enough. As a consequence, magnitudes/colours of clusters of similar ages and metallicities hosting AGB stars may display a large spread due to the effect of stochastic fluctuations in the number of bright, short-lived AGB stars, caused by the small, finite number of objects populating a real cluster. In other words, the integrated magnitudes/colours of star clusters with a small, stochastically fluctuating number of AGB stars, may take a large range of values that can be very different from the value calculated for a fully sampled AGB phase, with the number of stars appropriately scaled according to the AGB lifetime and the cluster total mass, in compliance with the Fuel consumption Theorem (Renzini & Buzzoni 1983).

Although the star clusters of the Magellanic Clouds are richer in stars than Galactic open clusters, stochastic

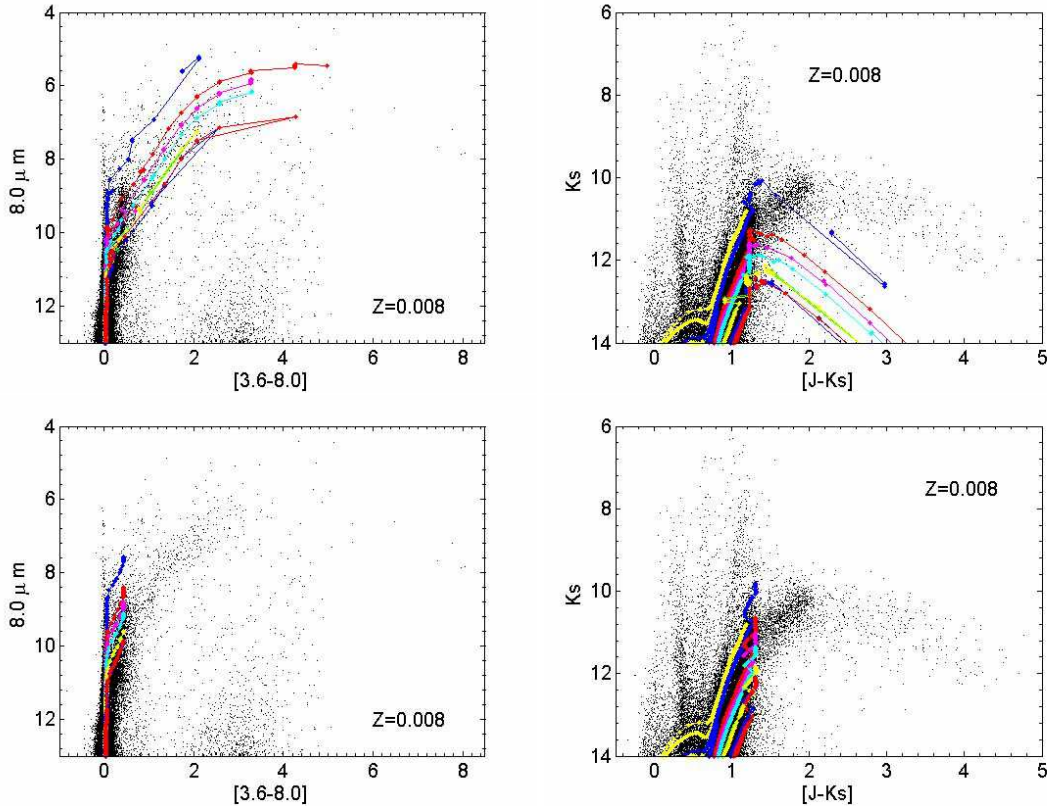


Figure 19. As Fig. 18, but for IRAC $[8 \mu\text{m}]$ vs $[3.6 - 8]$ CMDs (left panels) and K_s vs. $[J - K_s]$ (right panels).

effects can still be sizeable. Attempts to compare theory and observations by means of mean values of the integrated colours of clusters grouped into age bins (Noel et al. 2013), may lead to misleading results. Furthermore, the luminosity and effective temperature of stars during the TP-AGB phase vary significantly, affecting the colours by deviating from the mean, smoothed isochrone discussed in Sect. 2. This issue will be treated in detail in a forthcoming paper of this series (Salaris et al. 2013, in preparation).

The temporal variation of the integrated $[V - K_s]$ colours of LMC clusters is presented in Fig. 22. For the sake of clarity, the upper panel contains theoretical colour-age relations for $Z=0.004$, $Z=0.008$ and $Z=0.02$, while the lower panel shows the same but for SSPs with $Z=0.0001$ and $Z=0.0004$. Solid lines denote the case with dusty AGB stars, while dashed lines display dust-free results. Figure 23 shows the same comparisons but for the $[J - K_s]$ colour. The data have been selected (and plotted with different colours) according to their metallicity and age, the latter estimated by Pessev et al. (2006, 2008) from the cluster CMDs (see this paper for further details). Four age groups are considered. All these clusters have $[\text{Fe}/\text{H}] > -1.71$, therefore they can be classified as *metal-rich*. The data agree reasonably well with the theoretical age-colour relationships, in particular when appropriate metallicities for the clusters of the LMC are taken into account. This is displayed in the top panels of Figs. 22 and 23, for both the colours with and without dust around AGB stars, whereby the difference between the two cases starts when the first

AGB stars appear. Finally, we call attention to two 'bumps' toward redder colours displayed by the theoretical colour-age relationships: the first one occurs at an age of about 0.1 Gyr and is caused by the onset of the AGB phase; the colour becomes redder because of the increased flux in the near-IR pass-bands. The second 'bump' occurs at an age between 1 and 2 Gyr, and it is likely due to the development of the RGB phase; this is more evident when a higher metallicity is taken into account. See Chiosi, Bertelli & Bressan (1988), Girardi et al. (1995), and Bressan, Chiosi & Fagotto (1994) for a detailed discussion of the subject.

9.3 The colour-colour diagrams

Two-colour diagrams are powerful diagnostics of several photometric properties of star clusters (see Girardi et al. 1995, for a detailed discussion of the issue). Following Piovan, Tantaló & Chiosi (2003), we selected a small sample of clusters whose AGB population provides a strong contribution to the integrated light. These photometric data come from the *2MASS Second Incremental Data Release* and the *Image Atlas*, that contains 1.9 millions of images in the infrared bands J , H , and K_s . Pretto (2002) calculated the integrated magnitudes and made them available to us. Moreover, we considered the IR colours for the LMC and SMC clusters by Persson et al. (1983) used by Mouhcine (2002). As for their ages, we rely on the compilation by Pietrzynski & Udalski (2000), who presented age determinations for about 600 star clusters belonging to the cen-

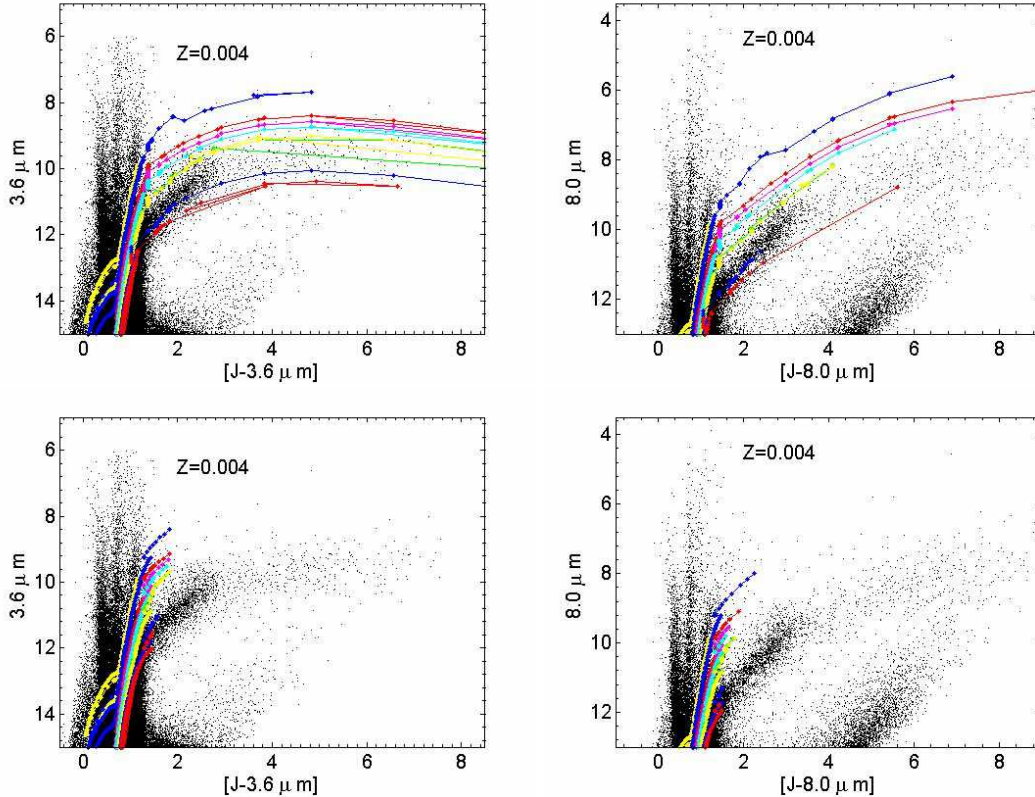


Figure 20. As Fig. 18, but for the SMC, using isochrones with $Z = 0.004$.

tral part of the LMC. They are younger than 1.2 Gyr, thus their AGB stars provide a major contribution to the integrated light. Figures 24, 25, and 26 display the two-colour diagrams $[H - K]$ vs. $[J - H]$, $[H - K]$ vs. $[V - K]$, and $[J - K]$ vs. $[V - K]$, respectively. Each diagram shows the data by Persson et al. (1983) for the LMC (open circles) and SMC (black stars), and the data by Pretto (2002) (cross-shaped points), all corrected for the reddening. The upper panel of each figure shows the new SSPs with (solid lines) and without (dashed lines) dust shells around AGB stars, whereas the lower panels display the old SSPs by Bertelli et al. (1994). For both types of SSPs, different metallicities are considered, namely $Z=0.02$ (magenta lines), $Z=0.004$ (black lines), and $Z=0.008$ (green lines); the age ranges goes from 100 Myr (when AGB stars start contributing to the integrated light of the stellar population) to 13 Gyr, when only low-mass AGB stars are present.

The new dusty SSPs cover the observed colour ranges better than both the old SSPs by Bertelli et al. (1994) (see Piován, Tantalo & Chiosi 2003, for more details) and the new ones without dust shells around AGB stars. The dust-free SSPs span a narrower range in $[H - K]$, while the new dusty SSPs extend over a larger $[H - K]$ interval and to bluer $[J - H]$ and $[V - K]$ colours. We recall that the $[V - K]$ colour is particularly suited to study the AGB phase of stellar populations. In fact the AGB phase greatly contributes to the NIR light of SSPs between ~ 100 Myr and ~ 1 Gyr, and causes abrupt changes in the NIR luminosity, while producing only small changes in the optical. Our new SSPs

extend towards bluer colours, approximately like the SSPs by Mouhcine (2002), as shown in Piován, Tantalo & Chiosi (2003). Differences between our SSPs and the models by Mouhcine (2002) are due to their adoption of empirical spectra for O- and C-stars, that are limited to the objects they observed, and do not cover the full range of relevant parameters (age, metallicity, $[C/O]$ -ratio). In our work we use instead theoretical spectra of M-stars, that cover all relevant parameters' range, but of course cannot match perfectly the empirical spectra. More work is required to improve the theoretical spectra of cool stars to be included in population synthesis studies.

It is interesting to compare colours that help to break the age-metallicity degeneracy. Following Pessev et al. (2008), we consider the $[B - J]$ vs. $[J - K]$ diagram. Puzia, Mobasher & Goudfrooij (2007) have shown that the colour $[B - J]$ is well suited for age estimates, while $[J - K]$ is more sensitive to metallicity (except for the small age interval around the onset of the AGB phase, where $[J - K]$ can show a weak age dependence). We again use the database by Pessev et al. (2006, 2008), considering the whole metallicity grid and ages from 10 Myr to 13 Gyr from our new dusty SSPs. Data and theoretical predictions are compared in Fig. 27. The age increases from left to right along the theoretical sequences. We consider here LMC and SMC clusters of any age, split into two groups: young ($t < 0.95$ Gyr) and old ones (age above this limit). Furthermore, we subdivide the clusters into *metal-rich* ($[Fe/H] > -1.71$), and *metal-poor* ones ($[Fe/H]$ above this limit).

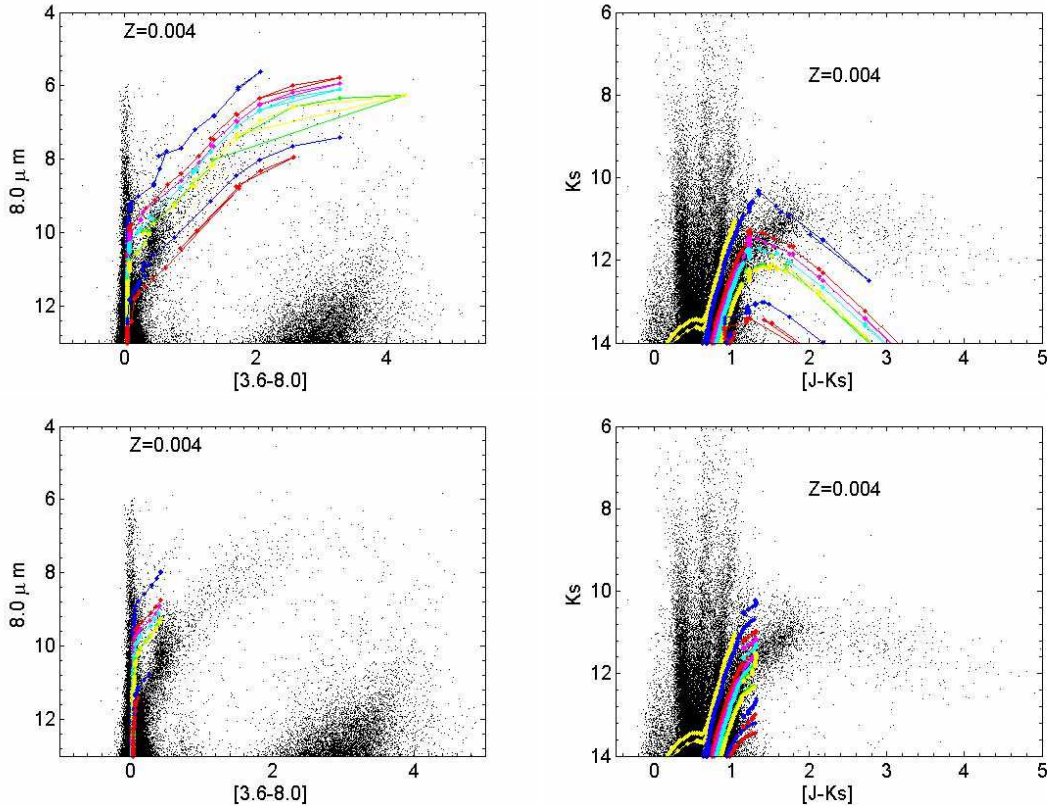


Figure 21. As Fig. 19, but for the SMC.

The open red circles denote young and metal-rich clusters, red stars display the old and metal-rich ones, and finally the black star denote the old and metal-poor objects. The upper panel shows the LMC clusters and the bottom panel the SMC ones. In case of the LMC we have clusters with all combinations of age and metallicity (only young metal poor clusters are lacking), while the SMC the database does not include any metal-poor object. There is a clear separation between the different age and metallicity groups: our theoretical colours overlap with the data, particularly in the region of the youngest metal-rich clusters. Instead, they fail to match the old clusters of the LMC between $0.3 \lesssim [B - J] \lesssim 0.6$ and $2 \lesssim [J - K] \lesssim 5$, that are mostly old metal-poor (even if some metal-rich clusters appear in this region). We encountered some problems also in the region between $1 \lesssim [B - J] \lesssim 1.3$ and $2 \lesssim [J - K] \lesssim 3$, populated by the oldest metal-rich clusters. Of course this partial disagreement with the observations suggests that some of the ingredients of the models should be improved, like the spectra for the cool stars in our stellar spectra library. It is however important to notice, as already pointed out, that stochastic fluctuations of the number of giant stars will always cause a spread of cluster colours at any age and metallicity. This effect is obviously amplified in case the SMC clusters, considering that we are analyzing *only* a very small number of objects. Stochastic fluctuations could explain the disagreement between data and theory in the above colour intervals as well.

9.4 Clusters of M31

Before concluding, we examine a sample of star clusters in M31, another Local Group galaxy, with a distance modulus of 24.47 mag (Holland 1998; Stanek & Garnavich 1998; McConnachie et al. 2005). M31 is the ideal Local Group galaxy to study globular clusters, for it contains more globulars than all other Local Group galaxies combined (Battistini et al. 1987; Racine 1991; Harris 1991; Fusi Pecci et al. 1993). The globular cluster system of M31 has been extensively studied over many decades (see Ma 2012, for a recent review of the subject). In the following we focus on clusters located in the outskirts of this galaxy, because they are useful probes of the substructures expected to form in the outer region of the host galaxy (Ma 2012), as predicted by the popular Λ CDM model for galaxy formation. This model predicts that these substructures continue to grow in time, from the accretion and the disruption of companions satellite.

We make use of the J , H , and K_s magnitudes from 2MASS imaging of 10 globular clusters in the outermost regions of M31, analyzed by Ma (2012). These data have been combined with V and I photometry (Galleti et al. 2004, 2006, 2007; Huxor et al. 2008). The sample of M31 halo globular clusters is taken from Mackey et al. (2006, 2007), who evaluated the metallicities ($-2.14 < [\text{Fe}/\text{H}] < -0.70$), distance modulus and reddening from their CMDs, using deep images obtained with ACS/*HST*. The cluster ages have been determined by Ma (2012), by comparing the integrated photometry with the SSP models by Bruzual & Charlot

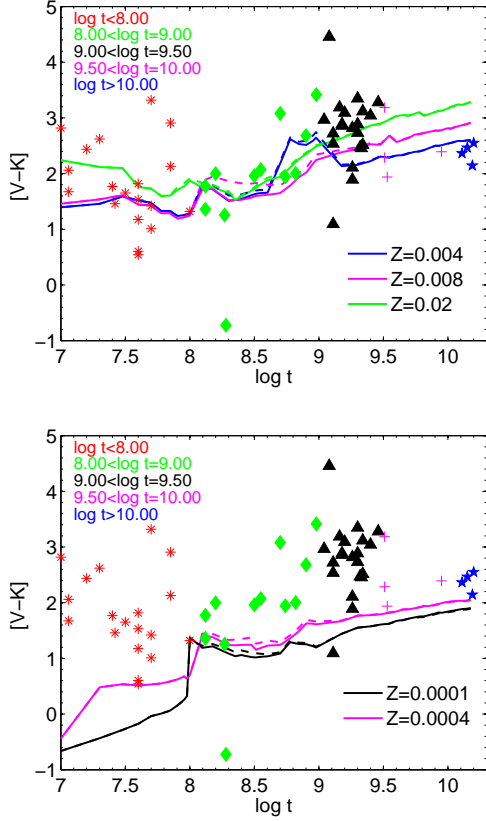


Figure 22. Upper panel: theoretical $[V - K_s]$ colours of our SSPs, with (solid lines) and without (dashed lines) the contribution of circumstellar dust shell around AGB stars, as a function of age (from 0.01 to 15 Gyr, with t in yr). We considered metallicities $Z=0.004$ (blue lines), $Z=0.008$ (magenta lines), $Z=0.02$ (green lines). The SSPs are superimposed on the integrated colours of LMC star clusters, taken from the compilation by Pessev et al. (2006, 2008); the data are plotted in different colours according to the cluster age, as labelled. Lower panel: as in the upper panel, but we superimposed SSPs of metallicity $Z=0.0001$ (black lines) and $Z=0.0004$ (magenta lines).

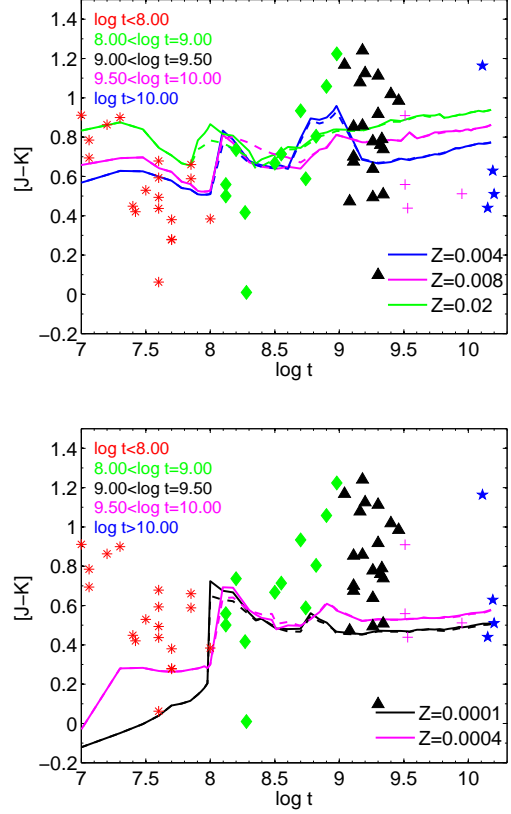


Figure 23. As Fig. 22, but for the $[J - K]$ colour.

(2003), based upon the Fagotto et al. (1994a,b,c) evolutionary tracks and a Salpeter IMF from $0.1M_{\odot}$ to $100M_{\odot}$. We adopt these age determinations, the same $[V - I]$ and $[J - K]$ colours and associated uncertainties, and compare these data to our SSPs with circumstellar dust around AGB stars. The upper panel of Fig. 28 displays the theoretical evolution of $[V - I]$ as a function of age, whereas the bottom panel does the same but for the $[J - K]$ colour. The $[V - I]$ colour appears best suited to match the age and metallicity of these clusters. Moreover, the uncertainties associated with the observational data are lower for this colour compared to $[J - K]$. As a last remark, we note that for some clusters Ma (2012) assigned a very old age, not only beyond the upper limit of our SSPs (this is not a problem because they can be easily extended), but more importantly well beyond the limit set by WMAP-5 data on the age of the Universe, e.g. 13.772 ± 0.059 Gyr (Dunkley et al. 2009).

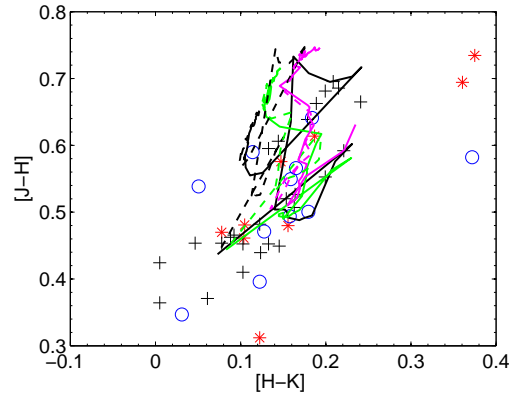


Figure 24. The *two colour diagram* $[H - K]$ vs. $[J - H]$ for young star clusters in the Magellanic Clouds. Open circles are LMC clusters selected by Mouhcine (2002) from the catalogue of Persson et al. (1983), while red stars denote the SMC counterpart. Cross-shaped points are LMC clusters whose IR colours have been collected by Pretto (2002) using 2MASS data. All data have been reddening corrected. The lines show the colour range spanned by the new SSPs with (solid lines) and without (dashed lines) the contribution of circumstellar dust shells. Results for different values of the metallicity are shown: $Z=0.02$ (magenta), $Z=0.004$ (black) and $Z=0.008$ (green). The range of SSP ages goes from 0.1 Gyr to 15 Gyr.

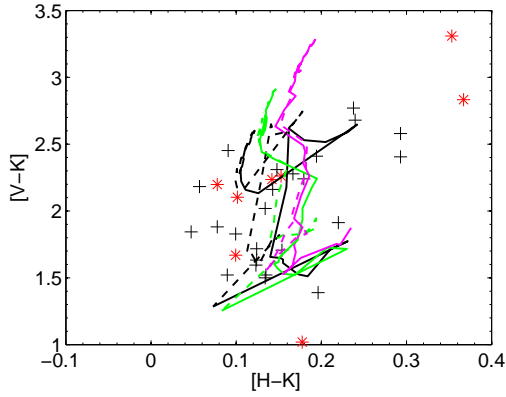


Figure 25. The same as in Fig. 24, but for $[H-K]$ vs. $[V-K]$ colours. The meaning of the symbols is the same as in Fig. 24.

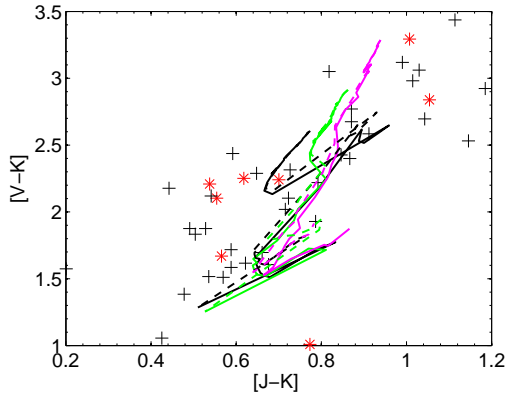


Figure 26. The same as in Fig. 24, but for $[J-K]$ vs. $[V-K]$ colours. The meaning of the symbol is the same as in Fig. 24.

10 SUMMARY AND CONCLUSIONS

Using state-of-the-art AGB models of low and intermediate-mass stars, and accounting for the effect on the model SED of dust shells surrounding the AGB central star, we have revised the Padua library of isochrones (Bertelli et al. 1994) to cover a wide range of chemical compositions (using a helium to heavy elements enrichment ratio $\Delta Y/\Delta Z = 2.5$) and ages.

The TP-AGB phase is taken from the detailed full evolutionary calculations by Weiss & Ferguson (2009). Two spectral libraries, containing about 600 dust enshrouded SEDs of AGB stars each, one for oxygen-rich M-stars and one for carbon-rich C-stars, have been calculated. Each library considers different values of the necessary input parameters (like the optical depth τ , dust composition, and temperature on the inner boundary of the dust shell). This is one of the few theoretical studies of stellar SEDs with dusty AGB stars, suitable for use in EPS models. The AGB star SEDs have been implemented into larger libraries of theoretical stellar spectra, to cover all relevant regions of the HRD where stars with a large range of initial stellar mass and chemical composition are found.

Starting from these isochrones and SEDs, we have cal-

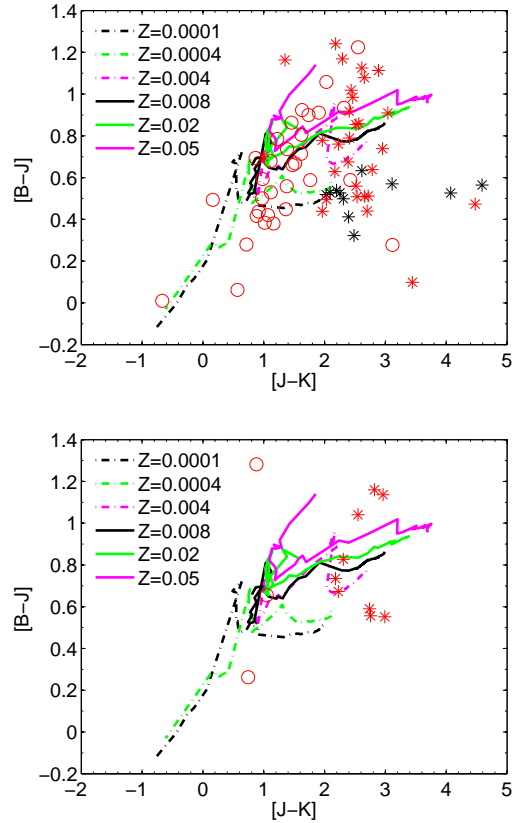


Figure 27. $[B-J]$ vs. $[J-K]$ diagrams for a sample of LMC (upper panel) and SMC (lower panel) star clusters. Three combinations of age and metallicity are considered: open red circles denote young ($t < 0.95$ Gyr) and metal-rich ($[Fe/H] > -1.71$) clusters, red stars denote old and metal-rich ones, and black stars display old and metal-poor objects. Superimposed on the data we show the new SSPs for different values of the metallicity, as labelled.

culated the integrated SED, magnitudes, and colours of SSPs with several different metallicities (6 values), ages (more than fifty values from ~ 3 Myr to 15 Gyr), and nine choices of the IMF.

The new isochrones and SSPs have been compared with CMDs of stellar populations in the LMC and SMC, with particular emphasis on the match to the observed AGB sequences. We also compared our theoretical predictions with integrated colours of star clusters in the same galaxies, using data from the SAGE catalogues (Blum et al. 2006; Bolatto et al. 2007), which match IRAC (or MIPS) data with 2MASS photometry. Finally, we have examined the integrated colours of star clusters located in the outskirts of M31.

The agreement between theory and observations is generally good, even if some discrepancies still occur. In particular, the new SSPs reproduce the very extended red tails of AGB stars in CMDs.

The whole libraries of spectra, isochrones and SSPs are made freely available to the scientific community, and can be obtained from the authors upon request.

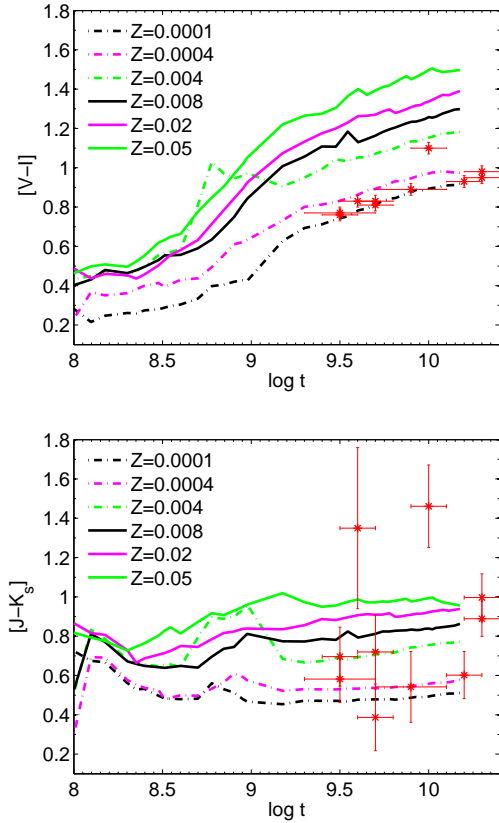


Figure 28. Theoretical evolution of the $[V-I]$ (upper panel) and $[J-K]$ (lower panel) colours as a function of age. SSPs for different metallicity are shown, as labelled. The time t is in yr. The data and their uncertainties are from Ma (2012).

11 ACKNOWLEDGMENTS

We would like to thank the anonymous referee whose comments improved the quality of the manuscript. We are deeply grateful to A. Buzzoni for fruitful discussions. L. P. Cassarà, L. Piovan and M. Salaris acknowledge the Max-Planck-Institut für Astrophysik (Garching - Germany) for the warm and friendly hospitality and the computational support during the visits when part of this study has been carried out. L. P. Cassarà is also grateful to P. Marigo for useful discussions, and to D. Maccagni and M. Polletta for their support. This study makes use of data products from 2MASS, which is a joint project of the University of Massachusetts and the Infrared Processing and Analysis Centre/California Institute of Technology, founded by the National Aeronautics and Space Administration and the National Science Foundation.

REFERENCES

Hempel M., Kissler-Patig M., 2004, *A&A*, 419, 863
 Allard F., Hauschildt P. H., 1995, *ApJ*, 445, 433
 Alongi M., Bertelli G., Bressan A., Chiosi C., Fagotto F., Greggio L., Nasi E., 1993, *A&AS*, 97, 851
 Aparicio A., Gallart C., 2004, *AJ*, 128, 1465
 Arimoto N., Yoshii Y., 1987, *A&A*, 173, 23

Aringer B., Girardi L., Nowotny W., Marigo P., Lederer M. T., 2009, *A&A*, 503, 913
 Battistini P., Bonoli F., Braccetti A., Federici L., Fusi Pecci F., Marano B., Borngen F., 1987, *A&AS*, 67, 447
 Begemann B., Dorschner J., Henning T., Mutschke H., Guertler J., Koempe C., Nass R., 1997, *ApJ*, 476, 199
 Bertelli G., Bressan A., Chiosi C., Fagotto F., Nasi E., 1994, *A&AS*, 106, 275
 Bertelli G., Girardi L., Marigo P., Nasi E., 2008, *A&A*, 484, 815
 Bertelli G., Girardi L., Nasi E., Marigo P., Castelli F., 2007, in *Astronomical Society of the Pacific Conference Series*, Vol. 374, *From Stars to Galaxies: Building the Pieces to Build Up the Universe*, Vallenari A., Tantalò R., Portinari L., Moretti A., eds., p. 41
 Bertelli G., Nasi E., Girardi L., Marigo P., 2009, *A&A*, 508, 355
 Bessell M. S., Brett J. M., Scholz M. W. P. R., 1991, *A&A*, 89, 335
 Bessell M. S., Brett J. M., Wood P. R., Scholz M., 1989, *A&AS*, 77, 1
 Bica E., Claria J. J., Dottori H., Santos, Jr. J. F. C., Piatti A. E., 1996, *ApJS*, 102, 57
 Blanco A., Borghesi A., Fonti S., Orofino V., 1998, *A&A*, 330, 505
 Blommaert J. A. D. L. et al., 2006, *A&A*, 460, 555
 Blum R. D., Mould J. R., Olsen K. A., Frogel J. A., Werner M., et al., 2006, *AJ*, 132, 2034
 Bolatto A. D. et al., 2007, *ApJ*, 655, 212
 Bouwens R., Bradley L., Zitrin A., Coe D., Franx M., et al., 2012, *ArXiv e-prints*
 Bressan A., Chiosi C., Fagotto F., 1994, *ApJS*, 94, 63
 Bressan A., Fagotto F., Bertelli G., Chiosi C., 1993, *A&AS*, 100, 647
 Bressan A., Granato G. L., Silva L., 1998, *A&A*, 332, 135
 Bruzual G., Charlot S., 2003, *MNRAS*, 344, 1000
 Buell J. F., 2012, *MNRAS*, 419, 2867
 Buzzoni A., 2002, *AJ*, 123, 1188
 Buzzoni A., 2005, *MNRAS*, 361, 725
 Carilli C. L. et al., 2001, *ApJ*, 555, 625
 Castellani M., Tornambe A., 1991, *ApJ*, 381, 393
 Chabrier G., 2003, *PASP*, 115, 763
 Chiosi C., Bertelli G., Bressan A., 1986, *Mem. Soc. Astron. Ital.*, 57, 507
 Chiosi C., Bertelli G., Bressan A., 1988, *A&A*, 196, 84
 Chung C., Yoon S.-J., Lee S.-Y., Lee Y.-W., 2013, *ApJS*, 204, 3
 Conroy C., 2013, *ArXiv e-prints*, 1301.7095
 Cordier D., Pietrinferni A., Cassisi S., Salaris M., 2007, *AJ*, 133, 468
 David P., Papoular R., 1990, *A&A*, 237, 425
 David P., Pegourie B., 1995, *A&A*, 293, 833
 Dickinson M., Stern D., Giallisco M., Ferguson H. C., Tsvetanov Z., et al., 2004, *ApJL*, 600, L99
 Dijkstra C., Speck A. K., Reid R. B., Abraham P., 2005, *ApJL*, 633, L133
 Dominik C., Sedlmayr E., Gail H., 1993, *A&A*, 277, 578
 Dotter A., Chaboyer B., Jevremović D., Kostov V., Baron E., Ferguson J. W., 2008, *ApJS*, 178, 89
 Draine B. T., 2009, *ArXiv:astro-ph/0903.1658*
 Dunkley J. et al., 2009, *ApJ*, 701, 1804
 Dwek E., Cherchneff I., 2011, *ApJ*, 727, 63
 Dwek E., Galliano F., Jones A., 2009, *ArXiv:astro-ph/0903.0006*
 Elitzur M., Ivezić Ž., 2001, *MNRAS*, 327, 403
 Elson R. A., Fall S. M., 1988, *AJ*, 96, 1383
 Elson R. A. W., Fall S. M., 1985a, *PASP*, 97, 692
 Elson R. A. W., Fall S. M., 1985b, *ApJ*, 299, 211
 Fagotto F., Bressan A., Bertelli G., Chiosi C., 1994a, *A&AS*, 104, 365
 Fagotto F., Bressan A., Bertelli G., Chiosi C., 1994b, *A&AS*, 105, 29

- Fagotto F., Bressan A., Bertelli G., Chiosi C., 1994c, *A&AS*, 105, 39
- Ferguson J. W., Alexander D. R., Allard F., Barman T., Bodnarik J. G., Hauschildt P. H., Heffner-Wong A., Tamanai A., 2005, *ApJ*, 623, 585
- Ferrarotti A. S., 2003, PhD thesis, Naturwissenschaftlich-Mathematische Gesamtfakultät der Universität Heidelberg, Germany. III + 143 pp. (2003)
- Ferrarotti A. S., Gail H., 2002, *A&A*, 382, 256
- Ferrarotti A. S., Gail H.-P., 2001, *A&A*, 371, 133
- Ferrarotti A. S., Gail H.-P., 2006, *A&A*, 447, 553
- Fluks M. A., Plez B., The P. S., de Winter D., Westerlund B. E., Steenman H. C., 1994, *A&AS*, 105, 311
- Fusi Pecci F., Cacciari C., Federici L., Pasquali A., 1993, in *Astronomical Society of the Pacific Conference Series*, Vol. 48, *The Globular Cluster-Galaxy Connection*, G. H. Smith & J. P. Brodie, ed., p. 410
- Gail H., Keller R., Sedlmayr E., 1984, *A&A*, 133, 320
- Gail H., Sedlmayr E., 1985, *A&A*, 148, 183
- Gail H., Sedlmayr E., 1999, *A&A*, 347, 594
- Gail H., Zhukovska S. V., Hoppe P., Tieloff M., 2009, *ApJ*, 698, 1136
- Gail H. P., Sedlmayr E., 1987, *A&A*, 171, 197
- Gall C., Andersen A. C., Hjorth J., 2011a, *A&A*, 528, A13+
- Gall C., Andersen A. C., Hjorth J., 2011b, *A&A*, 528, A14+
- Galletti S., Bellazzini M., Federici L., Buzzoni A., Fusi Pecci F., 2007, *VizieR Online Data Catalog*, 347, 10127
- Galletti S., Federici L., Bellazzini M., Buzzoni A., Pecci F. F., 2006, *ApJL*, 650, L107
- Galletti S., Federici L., Bellazzini M., Fusi Pecci F., Macrina S., 2004, *A&A*, 416, 917
- Galliano F., Dwek E., Chianal P., 2008, *ApJ*, 672, 214
- Gilman R. C., 1969, *ApJL*, 155, L185
- Gilman R. C., 1972, *ApJ*, 178, 423
- Girardi L., Bertelli G., Bressan A., Chiosi C., Groenewegen M. A. T., Marigo P., Salasnich B., Weiss A., 2002, *A&A*, 391, 195
- Girardi L., Bressan A., Chiosi C., Bertelli G., Nasi E., 1996, *A&AS*, 117, 113
- Girardi L., Chiosi C., Bertelli G., Bressan A., 1995, *A&A*, 298, 87
- Goebel J. H., Moseley S. H., 1985, *ApJL*, 290, L35
- Goudfrooij P., Alonso M. V., Maraston C., Minniti D., 2001, *MNRAS*, 328, 237
- Grassi T., Krstic P., Merlin E., Buonomo U., Piován L., Chiosi C., 2010, *ArXiv e-prints*
- Greggio L., Renzini A., 1990, *ApJ*, 364, 35
- Grevesse N., Noels A., 1993, *Physica Scripta Volume T*, 47, 133
- Groenewegen M. A. T., 1993, PhD thesis, Univ. of Amsterdam (1993)
- Groenewegen M. A. T., 1995, *A&A*, 293, 463
- Groenewegen M. A. T., 2006, *A&A*, 448, 181
- Groenewegen M. A. T., de Jong T., 1993, *A&AS*, 101, 267
- Groenewegen M. A. T., Whitelock P. A., Smith C. H., Kerschbaum F., 1998, *MNRAS*, 293, 18
- Habing H. J., 1996, *ARA&A*, 7, 97
- Habing H. J., Tignon J., Tielens A. G. G. M., 1994, *A&A*, 286, 523
- Hackwell J. A., 1972, *A&A*, 21, 239
- Harris W. E., 1991, *ARA&A*, 29, 543
- Heras A. M., Hony S., 2005, *A&A*, 439, 171
- Hofmeister E., Kippenhahn R., Weigert A., 1964, *Z. Astrophys.*, 59, 215
- Holland S., 1998, PhD thesis, The University of British Columbia (Canada)
- Huxor A. P., Tanvir N. R., Ferguson A. M. N., Irwin M. J., Ibata R., Bridges T., Lewis G. F., 2008, *MNRAS*, 385, 1989
- Iben, Jr. I., Renzini A., 1983, *ARA&A*, 21, 271
- Iben, Jr. I., Truran J. W., 1978, *ApJ*, 220, 980
- Iglesias C. A., Rogers F. J., 1996, *ApJ*, 464, 943
- Ivezic Z., Elitzur M., 1997, *MNRAS*, 287, 799
- Izzard R. G., Tout C. A., Karakas A. I., Pols O. R., 2004, *MNRAS*, 350, 407
- Jaeger C., Molster F. J., Dorschner J., Henning T., Mutschke H., Waters L. B. F. M., 1998, *A&A*, 339, 904
- Jonsson P., Groves B. A., Cox T. J., 2010, *MNRAS*, 403, 17
- Karakas A. I., 2011, in *Astronomical Society of the Pacific Conference Series*, Vol. 445, *Why Galaxies Care about AGB Stars II: Shining Examples and Common Inhabitants*, Kerschbaum F., Lebzelter T., Wing R. F., eds., p. 3
- Karakas A. I., Lattanzio J. C., Pols O. R., 2002, *Publications of the Astronomical Society of Australia*, 19, 515
- Kennicutt, Jr. R. C., 1998, *ApJ*, 498, 541
- Kitsikis A., Weiss A., 2007, in *Astronomical Society of the Pacific Conference Series*, Vol. 378, *Why Galaxies Care About AGB Stars: Their Importance as Actors and Probes*, Kerschbaum F., Charbonnel C., Wing R. F., eds., p. 99
- Kozasa T., Hasegawa H., 1987, *Progress of Theoretical Physics*, 77, 1402
- Kroupa P., 1998, in *Astronomical Society of the Pacific Conference Series*, Vol. 134, *Brown Dwarfs and Extrasolar Planets*, Rebolo R., Martin E. L., Zapatero Osorio M. R., eds., p. 483
- Kroupa P., 2007, *ArXiv Astrophysics e-prints*
- Larson R. B., 1998, *MNRAS*, 301, 569
- Lebzelter T., Posch T., Hinkle K., Wood P. R., Bouwman J., 2006, *ApJL*, 653, L145
- Lejeune T., Cuisinier F., Buser R., 1997, *A&AS*, 125, 299
- Lejeune T., Cuisinier F., Buser R., 1998, *A&AS*, 130, 65
- Lejeune T., Schaerer D., 2001, *A&A*, 366, 538
- Lorenz-Martins S., de Araújo F. X., Codina Landaberry S. J., de Almeida W. G., de Nader R. V., 2001, *A&A*, 367, 189
- Lorenz-Martins S., Lefevre J., 1994, *A&A*, 291, 831
- Lorenz-Martins S., Pompeia L., 2000, *MNRAS*, 315, 856
- Ma J., 2012, *Res. Astron. & Astrophys.*, 12, 115
- Mackey A. D. et al., 2006, *ApJL*, 653, L105
- Mackey A. D. et al., 2007, *ApJL*, 655, L85
- Madau P., Ferguson H. C., Dickinson M. E., Giavalisco M., Steidel C. C., Fruchter A., 1996, *MNRAS*, 283, 1388
- Marigo P., 2002, *A&A*, 387, 507
- Marigo P., Bressan A., Chiosi C., 1996, *A&A*, 313, 545
- Marigo P., Bressan A., Chiosi C., 1998, *A&A*, 331, 564
- Marigo P., Girardi L., 2001, *A&A*, 377, 132
- Marigo P., Girardi L., 2007, *A&A*, 469, 239
- Marigo P., Girardi L., Bressan A., Groenewegen M. A. T., Silva L., Granato G. L., 2008, *A&A*, 482, 883
- McConnachie A. W., Irwin M. J., Ferguson A. M. N., Ibata R. A., Lewis G. F., Tanvir N., 2005, *MNRAS*, 356, 979
- McDonald I. et al., 2011, *ArXiv e-prints*
- Meixner M., Gordon K. D., Indebetouw R., Hora J. L., Whitney B., et al., 2006, *AJ*, 132, 2268
- Messenger S. J., Speck A., Volk K., 2013, *ApJ*, 764, 142
- Michalowski M. J., Murphy E. J., Hjorth J., Watson D., Gall C., Dunlop J. S., 2010, *A&A*, 522, A15
- Michalowski M. J., Watson D., Hjorth J., 2010, *ApJ*, 712, 942
- Mouhcine M., 2002, *A&A*, 394, 125
- Narayanan D. et al., 2010, *MNRAS*, 407, 1701
- Nasi E., Bertelli G., Girardi L., Marigo P., 2008, *Memorie della Societa Astronomica Italiana*, 79, 738
- Noel N. E. D., Greggio L., Renzini A., Carollo M., Maraston C., 2013, *ArXiv e-prints*, 1305.3167
- Oesch P. A. et al., 2012, *ApJ*, 745, 110
- Ordal M. A., Bell R. J., Alexander R. W., Newquist L. A., Querry M. R., 1988, *Applied Optics*, 27, 1203
- Pégourié B., 1988, *A&A*, 194, 335
- Persson S. E., Aaronson M., Cohen J. G., Frogel J. A., Matthews K., 1983, *ApJ*, 266, 105

- Pessev P. M., Goudfrooij P., Puzia T. H., Chandar R., 2006, *AJ*, 132, 781
- Pessev P. M., Goudfrooij P., Puzia T. H., Chandar R., 2008, *MNRAS*, 385, 1535
- Pietrinferni A., Cassisi S., Salaris M., Castelli F., 2004, *ApJ*, 612, 168
- Pietrinferni A., Cassisi S., Salaris M., Castelli F., 2006, *ApJ*, 642, 797
- Pietrzyński G., Udalski A., 2000, *Acta Astronomica*, 50, 337
- Piovan L., Chiosi C., Merlin E., Grassi T., Tantaló R., Buonomo U., Cassarà L. P., 2011, *ArXiv e-prints*
- Piovan L., Tantaló R., Chiosi C., 2003, *A&A*, 408, 559
- Piovan L., Tantaló R., Chiosi C., 2006a, *MNRAS*, 366, 923
- Piovan L., Tantaló R., Chiosi C., 2006b, *MNRAS*, 370, 1454
- Pipino A., Fan X. L., Matteucci F., Calura F., Silva L., Granato G., Maiolino R., 2011, *A&A*, 525, A61
- Popescu C. C., Tuffs R. J., Dopita M. A., Fischera J., Kylafis N. D., Madore B. F., 2011, *A&A*, 527, A109+
- Portinari L., Sommer-Larsen J., Tantaló R., 2004, *MNRAS*, 347, 691
- Pretto T., 2002, Master's thesis, University of Padova, Italy
- Puzia T. H., Mobasher B., Goudfrooij P., 2007, *AJ*, 134, 1337
- Puzia T. H., Zepf S. E., Kissler-Patig M., Hilker M., Minniti D., Goudfrooij P., 2002, *A&A*, 391, 453
- Racine R., 1991, *AJ*, 101, 865
- Reimers D., 1975, *Memoires of the Societe Royale des Sciences de Liege*, 8, 369
- Renzini A., Buzzoni A., 1983, *Mem. Soc. Astron. Ital.*, 54, 739
- Renzini A., Voli M., 1981, *A&A*, 94, 175
- Robson I., Priddey R. S., Isaak K. G., McMahon R. G., 2004, *MNRAS*, 351, L29
- Rowan-Robinson M., 1980, *ApJS*, 44, 403
- Rowan-Robinson M., 2012, in *IAU Symposium*, Vol. 284, IAU Symposium, Tuffs R. J., Popescu C. C., eds., pp. 446–455
- Rowan-Robinson M., Harris S., 1982, *MNRAS*, 200, 197
- Salpeter E. E., 1955, *ApJ*, 121, 161
- Scalo J. M., 1986, *Fundam. Cosmic Phys.*, 11, 1
- Schönberner D., Steffen M., 2007, in *ASP Conference Series*, Vol. 378, *Why Galaxies Care About AGB Stars: Their Importance as Actors and Probes*, F. Kerschbaum, C. Charbonnel, & R. F. Wing, ed., p. 343
- Schutte W. A., Tielens A. G. G. M., 1989, *ApJ*, 343, 369
- Shapley A. E., Steidel C. C., Adelberger K. L., Dickinson M., Giallisco M., Pettini M., 2001, *ApJ*, 562, 95
- Silva L., Granato G. L., Bressan A., Danese L., 1998, *ApJ*, 509, 103
- Stanek K. Z., Garnavich P. M., 1998, *ApJL*, 503, L131
- Stanway E. R., Bunker A. J., McMahon R. G., 2003, *MNRAS*, 342, 439
- Steidel C. C., Adelberger K. L., Giallisco M., Dickinson M., Pettini M., 1999, *ApJ*, 519, 1
- Straniero O., Domínguez I., Cristallo S., Gallino R., 2003, *Proc. Astron. Soc. Aust.*, 20, 389
- Suh K.-W., 1999, *MNRAS*, 304, 389
- Suh K. W., 2000, *MNRAS*, 315, 740
- Suh K. W., 2002, *MNRAS*, 332, 513
- Tantaló R., Chinellato S., Merlin E., Piovan L., Chiosi C., 2010, *A&A*, 518, A43
- Tantaló R., Chiosi C., Bressan A., Marigo P., Portinari L., 1998, *A&A*, 335, 823
- Tielens A. G. G. M., 1990, in *From Miras to Planetary Nebulae: Which Path for Stellar Evolution?*, M. O. Mennessier & A. Omont, ed., pp. 186–200
- van den Bergh S., 1981, *A&AS*, 46, 79
- van Loon J. T., Cioni M., Zijlstra A. A., Loup C., 2005, *A&A*, 438, 273
- van Loon J. T., Groenewegen M. A. T., de Koter A., Trams N. R., Waters L. B. F. M., Zijlstra A. A., Whitelock P. A., Loup C., 1999, *A&A*, 351, 559
- van Loon J. T., McDonald I., Oliveira J. M., Evans A., Boyer M. L., Gehrz R. D., Polonski E., Woodward C. E., 2006, *A&A*, 450, 339
- van Loon J. T. et al., 1998, *A&A*, 329, 169
- Vassiliadis E., Wood P. R., 1993, *ApJ*, 413, 641
- Ventura P., D'Antona F., Mazzitelli I., 2002, *A&A*, 393, 215
- Wachter A., Schröder K.-P., Winters J. M., Arndt T. U., Sedlmayr E., 2002, *A&A*, 384, 452
- Wagenhuber J., Groenewegen M. A. T., 1998, *A&A*, 340, 183
- Wang R. et al., 2008a, *ApJ*, 687, 848
- Wang R. et al., 2008b, *AJ*, 135, 1201
- Waters L. B. F. M., Molster F. G., 1999, in *IAU Symp.* 191: *Asymptotic Giant Branch Stars*, Vol. 191, p. 209
- Waters L. B. F. M., Molster F. J., de Jong T., Beintema D. A., Waelkens C., et al., 1996, *A&A*, 315, L361
- Weiss A., Ferguson J. W., 2009, *A&A*, 508, 1343
- Weiss A., Schlattl H., 2008, *Astrophys. Space Sci.*, 316, 99
- Yamasawa D., Habe A., Kozasa T., Nozawa T., Hirashita H., Umeda H., Nomoto K., 2011, *ApJ*, 735, 44
- Zhang F., Han Z., Li L., Hurley J. R., 2002, *MNRAS*, 334, 883
- Zhang F., Han Z., Li L., Hurley J. R., 2004, *A&A*, 415, 117
- Zhang F., Han Z., Li L., Hurley J. R., 2005, *MNRAS*, 357, 1088
- Zhang F., Li L., Han Z., Zhuang Y., Kang X., 2012, *MNRAS*, 245
- Zhang K., Jiang B. W., Li A., 2009, *ApJ*, 702, 680
- Zheng W., Postman M., Zitrin A., Moustakas J., Shu X., et al., 2012, *Nat*, 489, 406
- Zhukovska S., Gail H.-P., 2008, *A&A*, 486, 229
- Zhukovska S., Gail H.-P., Tieloff M., 2008, *A&A*, 479, 453